GAMMA TOTAL IONIZING DOSE IMPACT ON THE CONTROL PERFORMANCE OF INTEGRATED POINT-OF-LOAD CONVERTERS

By

Patrick Clay Voytek

Thesis

Submitted to the Faculty of the

Graduate School of Vanderbilt University

In partial fulfilment of the requirements

for the degree of

MASTER OF SCIENCE

in

Electrical Engineering

August, 2014

Nashville, Tennessee

Approved:

Professor Arthur F. Witulski

Professor Robert A. Reed

ACKNOWLEDGMENT

I am very grateful to my advisor, Dr. Art Witulski, for his continual patience, guidance, and support throughout my research. I would like to thank him for teaching me that “the great tragedy of science is a beautiful theory murdered by an ugly fact” and that you must persevere in coming up with beautiful theories. His knowledge and wisdom has been invaluable to this effort. I would also like to thank Dr. Robert Reed for encouraging my interest in the CubeSat and Radiation Effects areas of study. Further, I would like to thank Rebekah Austin, Colin Thomas, Zachary Diggins, and the rest of the RER group for their help throughout this project and for allowing me to bounce ideas off of them. In particular, I would like to thank Colin for creating the Python code that was used in this project. I would also like to thank Martha Ingram and the O.H. Ingram Engineering Management Scholarship program for making it possible for me to be at Vanderbilt in the first place. I would also like to thank the DTRA robot grant "Analysis of Radiation-Induced Changes in Robotic Materials, Components, and Subsystems" grant number HDTRA1-13-1-0011 for providing the funding for the experimental parts and equipment purchased for this research effort. And finally, I would like to thank my friends and family for their efforts to maintain my sanity.

TABLE OF CONTENTS

Page

LIST OF TABLES

Table Page

LIST OF FIGURES

Figure Page

CHAPTER I

INTRODUCTION

The growing demand for electronics in radiation environments has driven the need for researching radiation effects on electronics. In some applications, mission critical tasks move the system into a radiation environment, such as the use of rescue robots in the event of a nuclear disaster [1]. In other applications, the purpose of the mission is to analyze the performance of internal electronics in the radiation environment, i.e. the many CubeSats that have provided relatively low-cost access to space in recent years [2]. In both cases, the components of the systems – sensors, actuators, communication equipment, etc. – need regulated DC power voltages. Clearly, if the power converter fails, its load will also stop operating. However, if the power regulator's output voltage drifts, then system performance can degrade in unexpected ways.

The gamma radiation experienced in a nuclear disaster or in the space environment will degrade the performance of the power regulators, also known as DC/DC converters, used for these applications. Many of them use commercial off the shelf (COTS) components [3], [4], [5]. These parts are not designed for use in a radiation environment, but they are significantly cheaper and easier to obtain quickly than "rad hard" components. The COTS integrated power converters that are commonly used are usually made from many MOS-based devices. It is well-known in the radiation effects community that MOS-based devices experience degradation due to the total ionizing dose (TID) of gamma radiation [6].

Linear regulators and DC/DC switching converters are two of the most common types of point of load (POL) DC/DC power converters [7]. Having one or two main bus

voltages – such as a battery voltage or a solar cell bus line – and many POL converters that provide a regulated voltage at the point of need allows for more flexibility in the system design. DC/DC switching power converters are frequently chosen because they provide a highly efficient regulated DC output voltage from the DC input voltage [7]. Historically, radiation effects research in the area of switching converters has focused on large signal changes and parametric shifts of subcomponents of converters built from discrete parts [8], [9]. Little information exists in the radiation effects literature about small-signal parameters or frequency response and stability of these converters. However, similar work has been done analyzing the loop gain for linear regulators [10]. Additionally, as technology scales, desired converters are increasingly integrated onto a single die. As the power regulation circuitry of these switching converters has become more compact, the ability to perform measurements on them has become more difficult. This thesis discusses the necessary measurement setup to perform small-signal measurements on integrated converters, the loop gain measurements that examine the effects of TID on a switching converter appropriate for the previously discussed applications, and a comparison of the results to Kelly's work on linear regulators [10]. Changes in the output regulation are correlated to changes in the loop gain and trends in the loop gain with increasing TID are discussed.

CHAPTER II

LOOP GAIN AND RELEVANT RADIATION EFFECTS BACKGROUND

Researching the effect of TID on the loop gain of switching converters requires an understanding of both control theory and radiation effects on electronics. The key background concepts necessary for this work are explained in this chapter.

Buck Converter Configuration

The buck converter is one of the most basic switching converter topologies. It takes an input DC voltage and produces a smaller, regulated DC output voltage. In switching converters, the value of the output voltage is adjusted by controlling the switch's duty cycle (D), the ratio of the on-time (t_{on}) of the switch over the switching period (T_s). By definition, this value is between 0 and 1, inclusive. For a buck converter the output voltage is related to the input voltage by the following equation:

$$V_{Out} = \frac{t_{on}}{T_s} V_{In} = D * V_{In} \quad (1)$$

Figure 1, from [7], shows the main components of the buck converter: a supply voltage (Vg), a switch (Q1), a diode (D1), an inductor (L1), an output capacitor (C), and a load (R) which create a DC output voltage V.

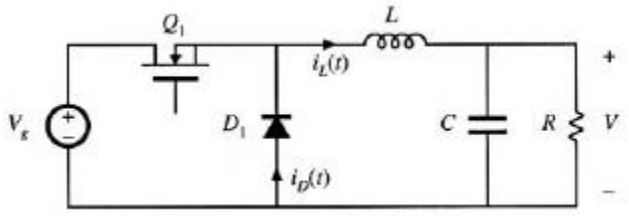

Figure 1. Buck Converter, image from [7]

In the buck converter while the switch (Q1) is closed, current ramps up through the inductor and voltage builds up across the capacitor. Then when the switch opens, the current through the inductor will decrease, decaying exponentially, while the voltage across the capacitor decays as well. If the inductor current never reaches zero, then the converter is said to be operating in the continuous conduction mode (CCM), and conversely if it does reach zero, then it is operating in the discontinuous conduction mode (DCM). Figure 2 and Figure 3 show the buck converter waveforms for CCM and DCM, respectively.

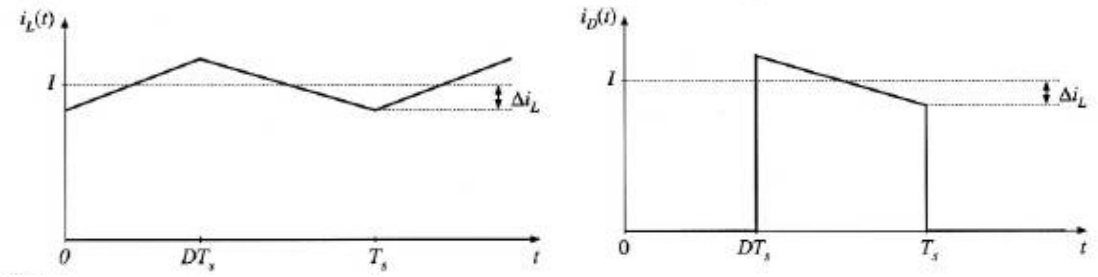

Figure 2. Inductor current (left) and diode current (right) of buck converter in CCM [7]

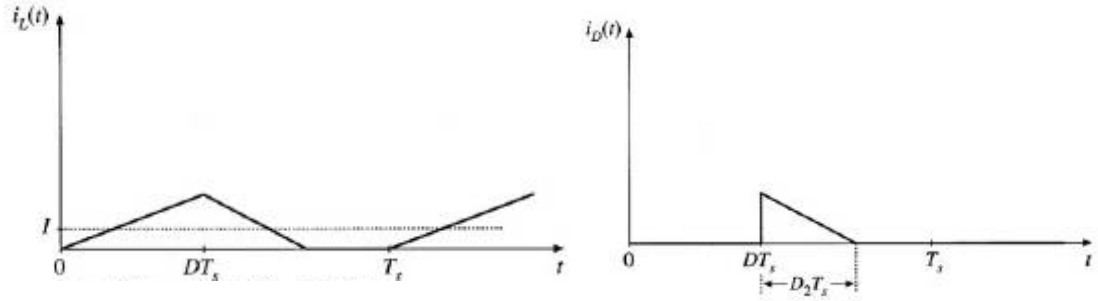

Figure 3. Inductor current (left) and diode current (right) of buck converter in CCM [7]

Figure 4 shows the buck converter, including the block diagrams for the control circuitry that provides the signal to drive the switch. It uses a resistor divider (shown as the sensor gain H(s) in Figure 4) to compare the value of the output voltage to a reference voltage and then adjust the duty cycle supplied by the pulse-width modulator (PWM).

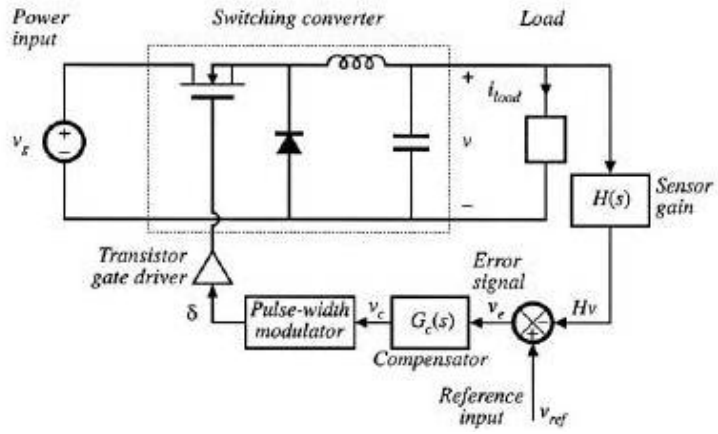

Figure 4. Buck Converter, block diagram [7]

Loop Gain Definition

The loop gain T(s) is defined as the product of the small-signal gains in the forward and feedback paths of the loop [7]. The magnitude of the loop gain determines how quickly a system will respond to a disturbance as well as how well the output tracks the reference. The loop gain affects performance of the regulator in terms of its bandwidth or cross-over frequency, (ω_c), as well as the steady-state error T(0). Figure 5 shows a classic feedback block diagram, with G as the open loop gain of the system, H as the gain of the feedback network, and e(s) as a disturbance, that illustrates the importance of having a large loop gain. Equation (2) shows how much each element contributes to the output voltage, and Equation (3) as discussed in [10] is the linear regulation of the feedback circuit, given that G(s) is the open loop line-to-output gain and T(s) is the loop gain of the feedback circuit.

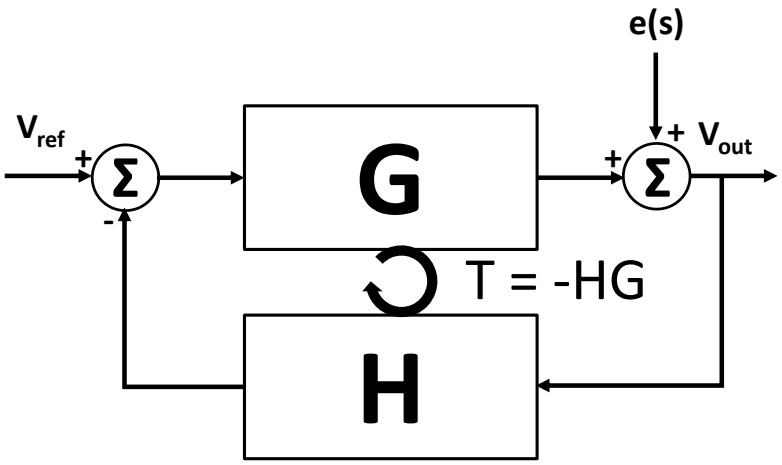

Figure 5. Feedback block diagram, including a disturbance e(s)

$$v_{out} = \frac{1}{H(s)}\frac{T(s)}{1+T(s)}v_{ref} + \frac{1}{1+T(s)}e(s) \tag{2}$$

$$\frac{v_{out}}{v_{\text{ref}}} = \frac{G(s)}{1+T(s)} \tag{3}$$

If the loop gain is sufficiently large, T(s) >> 1, then the disturbance will not have noticeable effect on the output voltage, which will track with the reference voltage. The ideal case of Equation (2) would be:

$$v_{out} = \frac{v_{ref}}{H(s)} \tag{4}$$

As the loop gain becomes smaller, the effects of the disturbance become bigger and the output voltage does not track with the reference voltage as well, as shown in Equation (2). Lumping the transfer functions into simple blocks provides an idealized example, but each component of the actual converter system has a transfer function which contributes to the overall response of the circuit and within a circuit these components will experience loading effects [11]. This loading effect leads to some of the measurement challenges, discussed in the next section.

A short discussion of loop gain has been provided here, but a further discussion of this control systems topic can be seen in most introductory-level control systems textbooks, such as [12].

Challenges of Loop Gain Measurement

There are many approaches to measuring the loop gain of a feedback system. In theory, it can be measured by opening the loop at an appropriate place, inserting a test signal, and measuring the ratio of the test signal and the signal that has gone around the loop [13]. Figure 6 is the classic image of this scenario, from Middlebrook's 1975 paper [13], which is still the basis for most modern loop gain measurement techniques. The voltage injection image is shown, but current injection can also be used in a similar fashion.

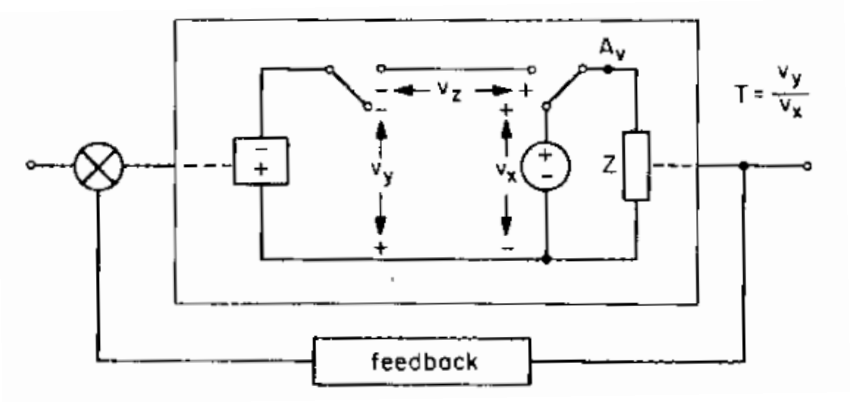

Figure 6. Open loop, loop gain measurement, using voltage injection from [13]

However, it is important that for true characterization of a circuit, the loop remain closed so that the bias points are not disturbed and so the system does not saturate on noise [13], [14]. Measurements made by breaking the loop do not account for the loading effects seen within a real circuit. Figure 7 is the classic image from [13], demonstrating loop gain measurement, using voltage injection, without breaking the loop. This requires

the use of a floating voltage source for injection (v_z in Figure 7), but this can be accomplished using a current probe as a 1 turn transformer.

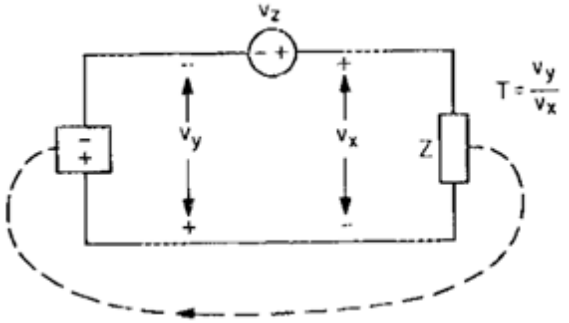

Figure 7. Closed loop, loop gain measurement, using voltage injection from [13]

In order to perform the measurement, a network analyzer with a variable frequency source and corresponding narrowband filter is used. Even assuming the appropriate equipment, the location of the injection point is also very important. For voltage injection the impedance seen looking "forward" (direction of control signal propagation) must be significantly greater than the impedance seen looking "backward" at the injection site. The reverse ratio must be true for a good current injection location [13]. This impedance requirement can be further complicated by the fact that measuring loop gain curves requires a sweep of the frequency of the injection signal. Since the injection site may have some reactive impedances, the variation of the frequency can change the impedance ratio seen at the injection location. For many applications, the injection point becomes inappropriate at high frequencies [14].

Radiation Environments

It is well-known that robots working on nuclear disasters will be exposed to high levels of radiation. One recent example is the Fukushima disaster of March 2011 [1] where rescue robots, which use COTS parts, had to be redesigned to withstand gamma

radiation for the duration of the mission [3], [4]. Similarly, satellites face high levels of radiation in the space environment [15]. Over the last 15 years, 200+ CubeSats have been launched [2], which has allowed access to space at significantly cheaper prices. However, part of the decrease in cost is because most of the components used are also COTS parts instead of space-qualified radiation hardened parts. This means that the parts are not designed to be "rad hard" to survive the space radiation environment and that testing must be done to determine which parts to select for CubeSat missions. The main radiation effects of concern in space are total ionizing dose (TID) [6], single event effects (SEEs) [16], and displacement damage [17]. This thesis focuses on the effects of TID on COTS DC/DC converters that could be used in these nuclear disaster rescue robots and CubeSats, so TID is discussed further in the following section. For more information on the other radiation effects, please see the given resources.

Total Ionizing Dose (TID) Overview

Extensive work has been done regarding the effects of TID on MOS-based devices [6]. It is well known that ionizing radiation creates electron-hole pairs within insulators, such as the gate-oxide of MOS-based devices, and that the subsequent interface and oxide traps are responsible for the parameter shifts seen by the devices. "The primary effects of ionizing radiation on power MOSFET's are changes in the threshold voltage and degradation of mobility. These effects result in slower switching speeds and reduced drive capability" [18]. Historically, research into TID effects on DC/DC converters has often focused on the power MOSFETs. They have larger gate oxides than other MOS transistors, which means they have larger charge collection volumes that make them more susceptible to TID. These same effects are experienced by

other MOS-based devices as well, just not to the same extent. Since COTS components are not designed to survive in the radiation environment, the gamma rays experienced in the previously discussed radiation environments will typically cause these effects in MOS-based devices.

Previous TID Regulator Research

Since DC/DC voltage regulators are crucial components of most electronics systems, examining the radiation response of DC/DC voltage regulators to TID is not a new area of research [8], [9], [10], [18], [19], [20]. Most previous work on switching converters has focused on the radiation response of the power MOSFETS [8], [18], [19] used in switching converters, but some has focused on the control circuitry [9]. All of this work has focused on device parameter changes or large signal performance changes in converters built from discrete components. The TID responses of underlying small signal parameters and the effects on integrated converters have been neglected thus far. However as shown in Figure 8, Andrew Kelly did examine the loop gain (an important small signal quantity for feedback circuits such as a DC/DC converter) of linear regulators, another type of voltage regulator [10]. Based on previous work [20], he focused on the error amplifier as the most sensitive element of the linear regulator to TID. He examined the total dose effects on the loop gain of four configurations of linear voltage regulator: a) NPN series, b) PNP series, c) NPN shunt, and d) PNP shunt. This thesis begins to fill the void of TID effects and measurement on an integrated converter including the small signal parameters of switching converters, by examining the effects of TID on the loop gain of the Max1951, a COTS buck converter.

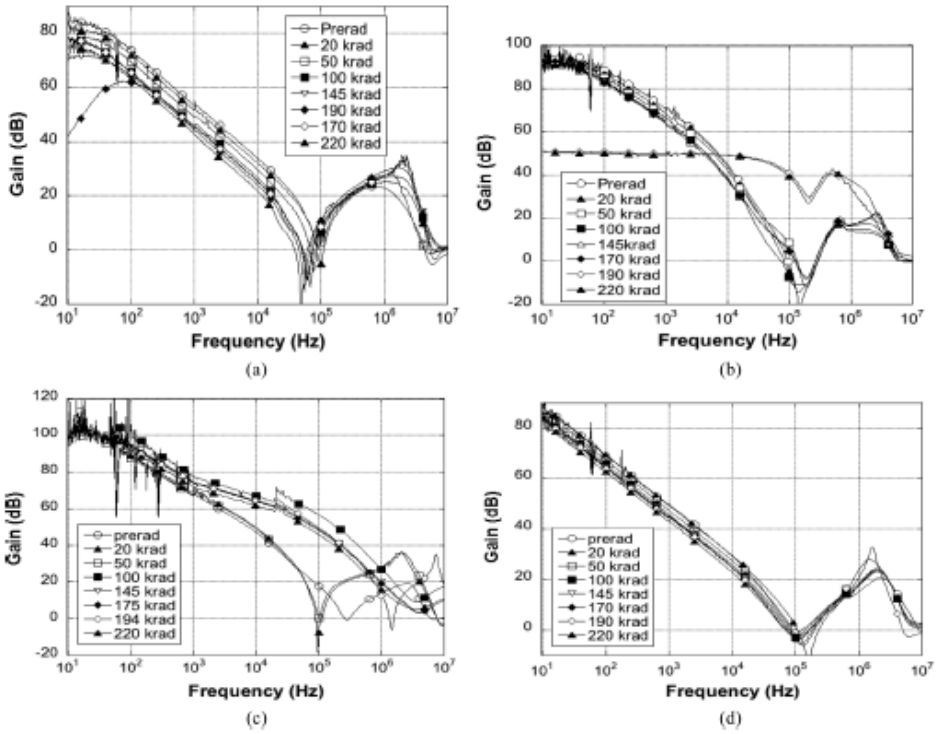

Figure 8. Total dose effects on loop gain of four configurations of linear regulator, from [7]

CHAPTER III

EXPERIMENTAL DESIGN

The Maxim1951A integrated converter was chosen as the buck converter to analyze for this study. It is a reasonable COTS DC-DC switching converter for both CubeSat and robotic efforts in space, and has been considered for CubeSat use in the past [21]. The design procedures available in the application note [22] were followed to analyze some potential factors on the effect of TID on buck converters. Schematics shown below, in Figure 10 and Figure 9, represent the circuits that were tested, and this chapter explains how the values in these configurations were selected. Unless otherwise noted, all equations come from the application note [22], are a rearrangement of those equations, or have values substituted into those equations.

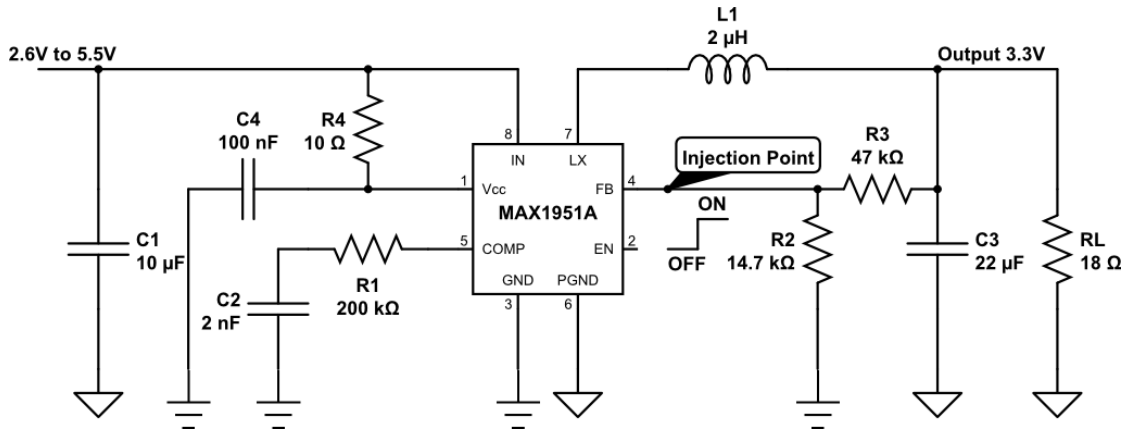

Figure 9. Max1951, nominally designed for 3.3 V output, Configuration 1

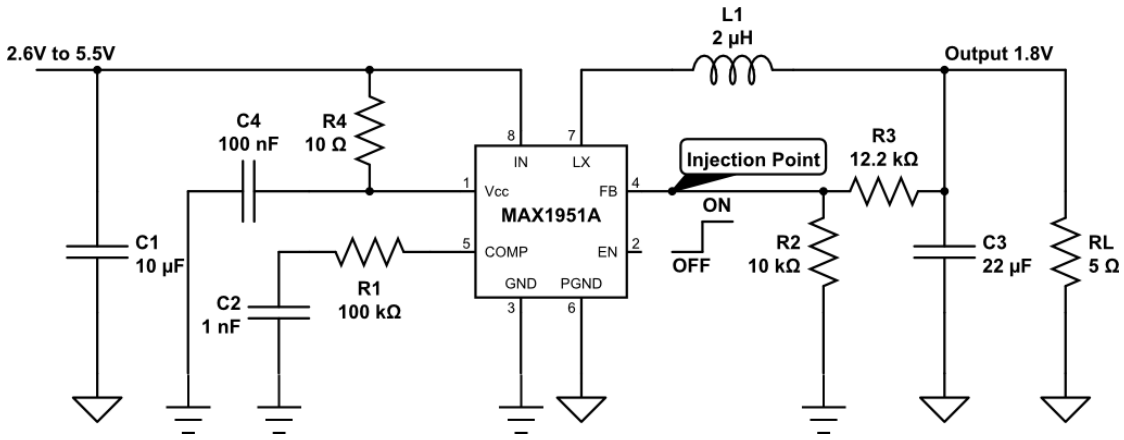

Figure 10. Max1951, nominally designed for 1.8 V output, Configuration 2

Output Voltage Selection

Two Maxim1951A buck converter configurations were designed to analyze the impact of the output voltage on the converter's TID sensitivity. The converters were nominally designed to produce the common digital outputs of 1.8 V and 3.3 V. The feedback resistors, R3 and R2 [22], can be determined from the following equation:

$$R3 = R2 \times \left[\frac{V_{Out}}{V_{FB}} - 1\right] \tag{5}$$

The feedback voltage, V_{FB}, is typically 0.8 V [21]. Designing for a nominal output voltage of 1.8 V:

$$\frac{R3}{R2} = \frac{1.8V}{0.8V} - 1 = 1.25 \tag{6}$$

Using standard 5% resistor values, choose R2 to be 10 kΩ and then find the closest available resistor values for R3.

$$\frac{R3}{R2} = \frac{(10+2.2)\,k\Omega}{10k\Omega} = \frac{12.2k\Omega}{10k\Omega} = 1.22 \tag{7}$$

Next, calculate the theoretical output voltage, using these resistor values.

$$V_{Out} = V_{FB} \times \left[\frac{R3}{R2} + 1\right] = 0.8V \times \left[\frac{12.2k\Omega}{10k\Omega} + 1\right] = 1.776\,V \approx 1.8\,V \tag{8}$$

The designed output voltage for the first set of Max1951 converters is 1.8 V, using a R2 of 10 kΩ and a R3 of 12.2 kΩ . Now the same process can be followed for a desired, nominal output of 3.3 V. The calculated R2 for this converter configuration is 14.7 kΩ, a 10 kΩ resistor in series with a 4.7 kΩ resistor, and the calculated R3 is 47 kΩ. Thus, the designed output voltage for the other configuration of Max1951 converters is approximately 3.4 V.

Load Resistor Selection

The goal of this experiment is to analyze the changes in the loop gain, and since changes in the converter mode of operation will change the loop gain, the experiment was designed to avoid operation in supervisory modes. Since the Max1951 has multiple supervisory modes [22], a relatively low output power was chosen that should not cause the part to current limit or engage thermal-overload protection. One factor that could cause two converters to have different responses to TID is to have different output voltages because this corresponds with a different duty cycle [7], meaning the portion of time during operation that the MOS devices are biased on is different. It is well-known in the radiation effects community that an NMOS device is more sensitive to TID when it is biased with a field across the oxide. It has been shown that in a buck converter, the switching device's radiation response varies based on the bias condition – positive, grounded, or switching – so the circuit is biased in its operable state during irradiation to provide the most realistic results [8], [18]. As such, two configurations of the Max1951 were tested, designed for different output voltages, but with the output power maintained approximately equal. A comparison of the output power for both configurations is shown below, in Table 1.

Table 1. Configuration Comparison

	Configuration 1	Configuration 2
Output Voltage (V)	3.4	1.8
Load Resistance (Ohm)	18	5
Output Current (mA)	189	360
Output Power (mW)	642	648

Thermal Considerations

Since the Max1951 has thermal-overload protective circuitry [22], the load resistance was designed to keep the output power small enough to avoid this supervisory mode. The thermal admittance of the 8-Pin SO package was given as 12.2 mW/^{o}C [22], which gives the following thermal resistance:

$$R_{\theta} = \frac{1}{12.2\times10^{-3}} = 82.0℃/W \tag{9}$$

Using the Ohm's Law equivalent for heat flow, with T as temperature and P as dissipated power, and the absolute maximum rating for continuous power dissipation [22], the maximum recommended junction temperature for continuous operation can be calculated, as shown in Figure 11 and Equations (10)-(12).

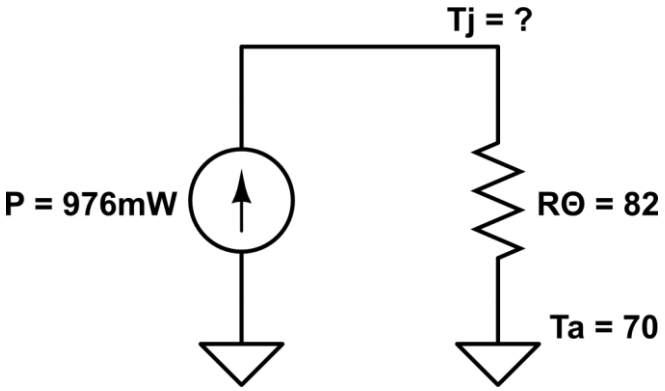

Figure 11. Thermal model, maximum recommended junction temperature for continuous operation

$$\Delta T = P \times R_\theta \tag{10}$$

$$T_{j,Max} - T_A = P_{Max} \times R_\theta \tag{11}$$

$$T_{j,Max} = (976 \times 10^{-3}\text{W} \times 82.0\text{℃/W}) + 70\text{℃} \tag{12}$$

This yields a maximum recommended junction temperature ($T_{j,Max}$) for continuous operation of 150 degrees Celsius. Next, the continuous output power (P_{Max}) that would create this junction temperature with an ambient temperature, T_A, of 25 degrees Celsius is calculated as shown in Figure 12 and using Equation (13), by rearranging Equation (11).

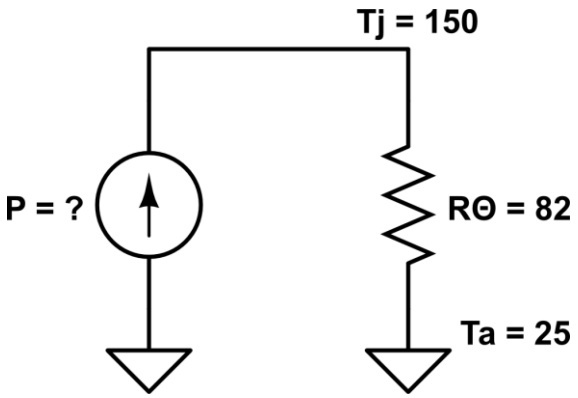

Figure 12. Thermal model, maximum recommended output power for continuous operation

$$P_{Max} = \frac{T_{j,Max} - T_A\ ℃}{R_\theta} = \frac{150 - 25\ ℃}{82.0\ ℃/W} \tag{13}$$

This yields a maximum recommended output power for continuous operation of roughly 1.52 W. This is well below the operating power of both configurations, so if the assumption of a 25 degree ambient operating temperature is valid, then the thermal-overload protection circuitry should not be a problem.

Output Inductor Design

Following the design suggestions of the application data sheet [22], a 2 μH inductor was chosen. To see a calculation of more ideal inductor values that could be used for further testing, see Appendix A.

Continuous and Discontinuous Conduction Modes

Based on the mode of operation, the loop gain will change. As such, both continuous and discontinuous modes of operation are examined in this experiment. Continuous conduction mode (CCM) occurs when half of the peak-to-peak current is less than the DC current, and discontinuous conduction mode (DCM) occurs otherwise. Equation (14) [7] provides the current ripple magnitude, which must be less than half of the DC current for the converter to be in CCM, as shown in Figure 13. Equations (14)-(19), from [7], provide the criteria for determining whether or not a buck converter is in CCM or DCM.

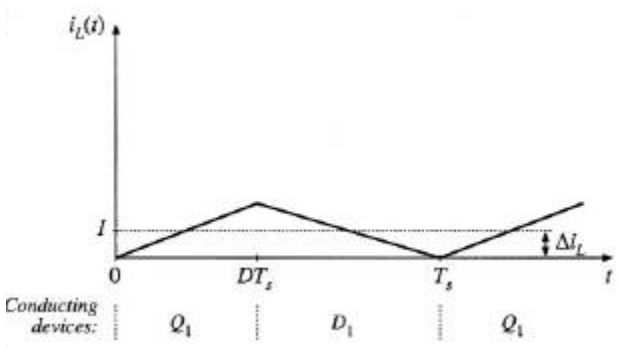

Figure 13. Buck converter inductor current at the boundary between CCM and DCM [7]

$$\Delta i_L = \frac{V_{In} - V_{Out}}{2L} DT_s = \frac{V_{In} DD'T_s}{2L} \tag{14}$$

$$I > \Delta i_L \qquad \text{for CCM} \tag{15}$$

$$\frac{DV_{In}}{R} < \frac{DD'T_s V_{In}}{2L} \qquad \text{for DCM} \tag{16}$$

$$R_{crit}(D) = \frac{2L}{D'T_s} \tag{17}$$

$$R > R_{crit}(D) \qquad \text{for CCM} \tag{18}$$

$$R < R_{crit}(D) \qquad \text{for DCM} \tag{19}$$

Using the facts that the duty cycle of a buck converter is equal to the output voltage divided by the input voltage and that the switching period T_s is equal to the inverse of the switching frequency, Equation (20) provides the R_{crit} for this experiment. Equations (21) and (22) provide the R_{crit} values for Configuration 1 and Configuration 2, respectively.

$$R_{crit}(D) = \frac{2Lf_{sw}}{\left(1 - \frac{V_{Out}}{V_{In}}\right)} \tag{20}$$

$$R_{crit\,1}(D) = \frac{2*2*10^{-6}*10^{6}}{\left(1 - \frac{3.4}{5}\right)} = 12.5\Omega \tag{21}$$

$$R_{crit\,2}(D) = \frac{2*2*10^{-6}*10^{6}}{\left(1 - \frac{1.8}{5}\right)} = 6.25\Omega \tag{22}$$

As seen in Table 1, Configuration 1 has a load resistance of 18 ohms and Configuration 2 has a load resistance of 5 ohms. This means that Configuration 1 should operate in CCM and Configuration 2 should operate in DCM.

Compensation Design

Most voltage-mode controllers require an elaborate compensation network to stabilize the control loop, but the Max1951A uses a current-mode control scheme that simplifies the compensation network [22]. This section provides the math used to determine the compensation design for R1 and C2, which was determined by following the direction of the application note [22]. The power modulator, output feedback divider and error amplifier form the basic regulator loop, which makes the loop-gain equation at the unity-gain frequency [22]:

$$G_{EA(fc)} \times G_{MOD(fc)} \times G_{FB} = 1 \quad (23)$$

$G_{EA(fc)}$ is the gain of the transconductance amplifier at the crossover frequency (f_C), $G_{MOD(fc)}$ is the gain of the power modulator at f_C, and G_{FB} is the gain of the feedback divider. Equation (24) shows the calculation of $G_{EA(fc)}$, with gm_{EA} being a constant given in the application note, equal to 60 μS. Equation (25) shows the calculation of $G_{MOD(fc)}$, with g_{mc} being a constant given in the application note equal to 4.2 S, R_{LOAD} being the load resistance, and f_{pMOD} being the modulator pole frequency caused by the output capacitor along with its equivalent series resistance and the load resistance. G_{FB} is just the ratio of the feedback voltage, which is 0.8 V, as shown in Equation (26). The equation for f_{pMOD} is given in the application note and is shown in Equation (27). As per the application note, for a 2 μH output inductor, the closed-loop unity gain crossover frequency is set at 200 kHz [22].

$$G_{EA(fc)} = gm_{EA} \times R_1 \tag{24}$$

$$G_{mod(fc)} = g_{mc} \times R_{Load} \times f_{pMOD}/f_C \tag{25}$$

$$G_{FB} = \frac{V_{FB}}{V_{OUT}} \tag{26}$$

$$f_{pMOD} = \frac{1}{2\pi \times C_{Out} \times (R_{Load} + R_{ESR})} \tag{27}$$

Substitution into Equation (23) creates Equations (28) which can be used to determine the necessary value of the compensation resistor, but a correction factor is needed to account for the extra phase introduced by the current loop at frequencies above 100kHz. K is this correction factor and is given to be 0.47 for an output capacitor of 22 μF [22]. Equation (29) sets the error-amplifier compensation zero formed by R1 and C2 at the modulator pole frequency at maximum load [22]. Due to an inconsistency in the application note between its original stated equation for C2 and the equation used in its sample calculation, another Maxim application note for a similar product (Max1951/Max1952) [23] was used to verify Equation (29). These equations are used to determine the necessary compensation resistor and capacitor for each configuration.

$$R_1 = \frac{V_{Out} \times K}{g_{mEA} \times V_{FB} \times G_{mod\ (fc)}} \tag{28}$$

$$C_2 = \frac{V_{Out} \times C_{Out}}{R_1 \times I_{Out\ (Max\ )}} \tag{29}$$

Equations (30)-(33), from [22], were used to calculate the appropriate values for Configuration 1, which has a theoretical output voltage of 3.4 V across an 18 ohm load. For calculations involving the equivalent series resistance (ESR) of ceramic capacitors that did not provide their ESR, a value of 0.01 ohms was assumed, based on available information.

$$f_{pMOD} = \frac{1}{2\pi(22 \times 10^{-6} F)(18 + 0.01)} = 402\ Hz \tag{30}$$

$$G_{mod\,(fc)} = 4.2 \times 18 \times \frac{402Hz}{200kHz} = 0.152 \quad (31)$$

$$R_1 = \frac{3.358 \times 0.47}{(60 \times 10^{-6})(0.8)(0.152)} = 216319\Omega \approx 200k\Omega \quad (32)$$

Selecting the nearest available 5% resistor value, 200 kilohms is selected for R1.

$$C_2 = \frac{(3.358V)(22 \times 10^{-6}F)}{(200k\Omega)(\frac{3.358V}{18\Omega})} = 1.98 \times 10^{-9}F \approx 2nF \quad (33)$$

Selecting the nearest readily available capacitor value, 2 nF is selected for C_2. Equations (34)-(37), from [22], were used to calculate the appropriate values for Configuration 1, which has a theoretical output voltage of 1.8 V across a 5 ohm load.

$$f_{pMOD} = \frac{1}{2\pi(22 \times 10^{-6}F)(5+0.01)} = 1443.98Hz \approx 1.44\ kHz \quad (34)$$

$$G_{mod\,(fc)} = 4.2 \times 5 \times \frac{1.44kHz}{200kHz} = 0.151 \quad (35)$$

$$R_1 = \frac{1.8 \times 0.47}{(60 \times 10^{-6})(0.8)(0.151)} = 116722\Omega \approx 100k\Omega \quad (36)$$

Selecting the nearest available 5% resistor value, 100 kilohms is selected for R1.

$$C_2 = \frac{(1.776V)(22 \times 10^{-6}F)}{(100k\Omega)(\frac{1.776V}{5\Omega})} = 1.1 \times 10^{-9}F \approx 1nF \quad (37)$$

Selecting the nearest readily available capacitor value, 1 nF is selected for C_2.

Design for Measurement

The circuits were designed with the intent to perform measurements of the loop gain, impedance at the injection point, operating mode, and output DC voltage. To allow for signal injection via a small transformer into the circuit for the transfer function measurements, a wire loop was included between the FB pin and the components connected to it. This point was selected as the injection point to meet the criteria for approximating an ideal injection point as discussed by Middlebrook [13], because the

impedance seen looking into the FB pin should be high, relative to the components attached to it. Figure 14 is the functional diagram of the Max1951A, which shows that the impedance looking into the FB pin will see the impedance of an input terminal of a transconductance amplifier. Looking into a transconductance amplifier should have a relatively high impedance, but this may not be true over all frequencies. Headers were included at both ends of the injection wire to allow for verification of the impedance looking into the FB pin and measurement of the loop gain. A small loop of wire was included between the inductor and the output node for measurement of the inductor current and another header was included at the LX pin to monitor the mode of operation of the converter. No additional ground connections were made since connections to the ground plane could be made through the ground banana plug. Output DC voltage could be measured at the load resistor of each circuit, so no additional output headers were included either. Figure 15 shows the location of each of the measurement points.

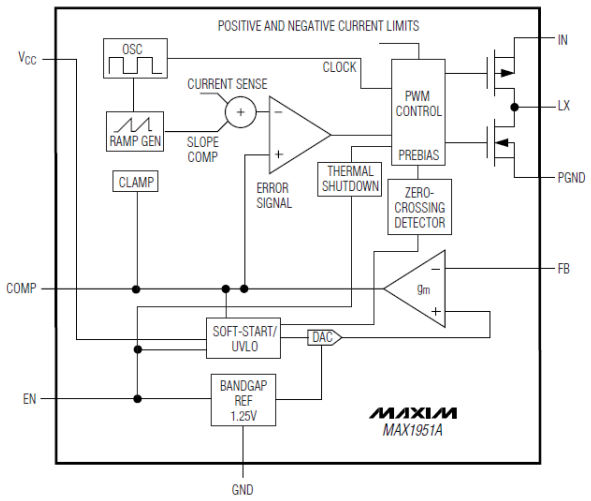

Figure 14. Max1951 functional diagram [21]

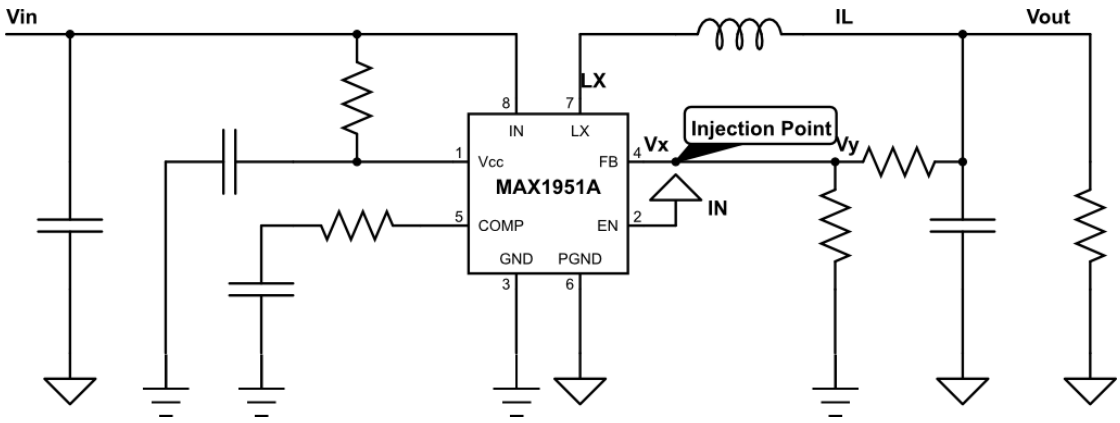

Figure 15. Max1951 measurement locations for Vy, Vx, LX, IL, and Vout

CHAPTER IV

EXPERIMENTAL SETUP

This chapter provides the test setup that was used to obtain all data presented in this paper. The loop gain, impedance at the injection point, operating modes, and line regulation of the converters were examined between iterative rounds of TID. Three copies of each configuration were built and tested all on the same board, with BNC connectors used as high-power switches to allow all of them to run on the same power supply during irradiation but be tested separately. Figure 16 shows the schematic and Figure 17 shows picture of this test board. For further information on the construction of this test board, see Appendix B.

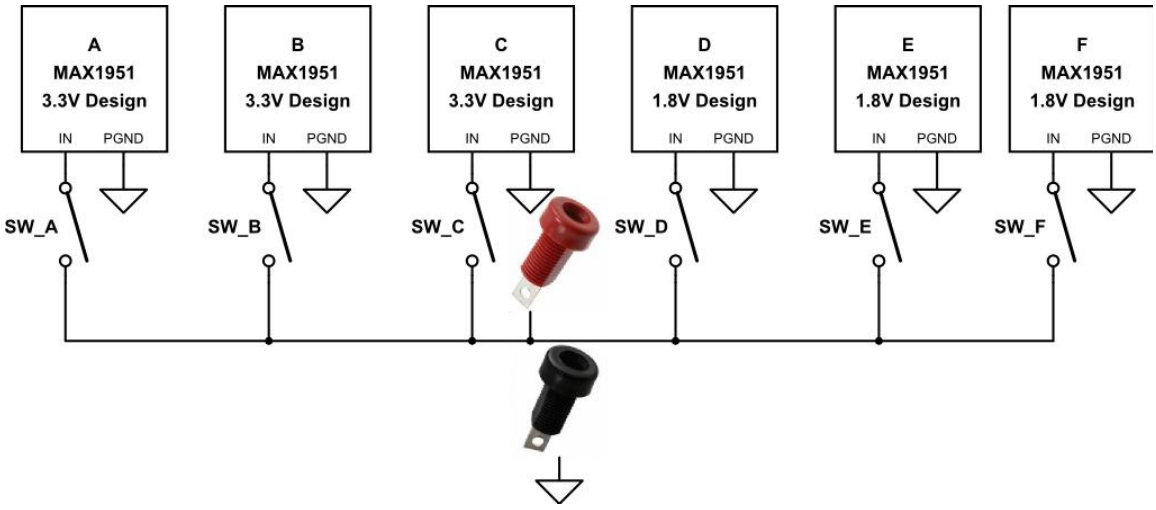

Figure 16. Test circuit board schematic

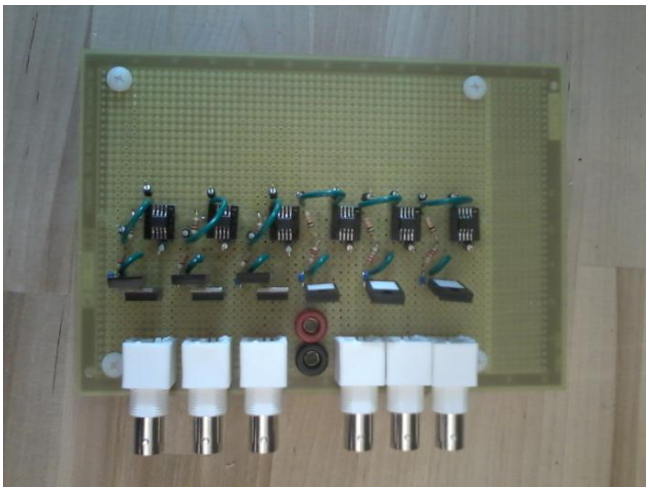

Figure 17. Test circuit board picture

Radiation Environment

Data in this thesis was obtained after each dose step in a Cs-137 irradiator. See Appendix C to see further information about the half-life calculator that was used to determine the dose rate. The test board was placed at a measured distance of 12.5 cm from the source in a clamp to ensure a consistent distance for all radiations, as shown in Figure 18. Then the dose rate at that distance along with the time spent under irradiation was used to determine the total accumulated dose. A pathfinder test was conducted, in which the converter failed around 80 krad (Si). The typical dose of interest is krad (SiO_2) since the effects of TID are due to the energy that is deposited in the oxide rather than the semiconductor. However, information for this thesis has been reported in krad (Si) since the source was calibrated as such. To see more information on the calibration, see Appendix C. To convert from krad (Si) to krad (SiO_2), use Equation (38), from [10].

$$1.8\, rad(Si) = 1.0\, rad\, (SiO_2) \tag{38}$$

Using this information, the dose steps for this experiment were spread logarithmically up to 80 krad (Si), with 5 krad (Si) steps taken after that to get more

information shortly before failure. See Appendix D for the MATLAB code that was used to determine the logarithmic spread of the dose steps. Table 2 provides the total dose information for this test.

Figure 18. Irradiation setup in the Shepard Cell Irradiator

Table 2. TID information for 12.5 cm from the Cs-137 source on June 2, 2014

Dose Rate:	283.1	rad/min
Total Dose (krad [Si])	Total Irradiation Time (Min.)	Irradiation Step (Min.)
1	3.53	3.53
2	7.06	3.53
4	14.13	7.06
9	31.79	17.66
19	67.11	35.32
39	137.76	70.65
80	282.59	144.83
85	300.25	17.66
90	317.91	17.66

During irradiation, all of the BNC shorts were in place and a GW Instek GPD-4303S Power Supply along with two banana to banana cables were used to provide 5 V to all of the converters. This biased the converters "on" so that the internal devices were switching during irradiation.

Measurement Setup

The following measurements were taken outside of the irradiator. The measurements of the impedance at the injection point were taken prior to irradiation, and the rest were taken prior to irradiation as well as iteratively between doses of irradiation.

Loop Gain Measurement

After each dose step, the power supply was turned off and the test board was removed from the irradiator. Next, BNC shorts B-F were removed so that Circuit A could be analyzed. Then, the power supply was reconnected and turned back on to supply 5V to the circuit under test. The Agilent 4395A Network Analyzer along with two Tektronix P2221 Voltage Probes and one Tektronix P6022 AC Current Probe were used to perform a loop gain measurement. The current probe was attached to the RF output of the Network Analyzer to act as the floating small-signal injection source, v_z, as in Figure 7, recopied below as Figure 19. The current probe wrapped around the wire between the FB pin and the other components, being used as a one-turn transformer to inject a small-signal voltage into the circuits, at the injection points shown in Figure 15, recopied below as Figure 20. The voltage probes were attached to the header's on either side of the injection wire and through Agilent 41802A 1MOhm Adapters to the Network Analyzer's inputs A and B. Both probes were set to 10x in order to reduce the capacitive load, since the 10x factors divide back out and do not affect the loop gain. The Network Analyzer

was set to record both the magnitude of the loop gain and its phase, with a logarithmic sweep of 201 points across a start frequency of 500 Hz to a stop frequency of 500 kHz. The source power was 0 dBm and the IF bandwidth was 10 Hz. Once this measurement was completed, the power supply was turned off, the BNC connector was removed from the previous circuit and the following circuit's BNC connector was put in place, and then the same measurement was performed on each of the subsequent circuits B-F.

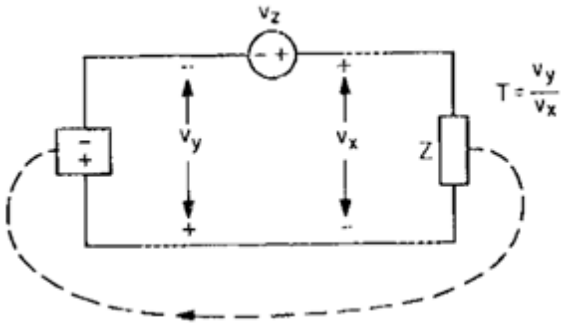

Figure 19. Closed loop, loop gain measurement, using voltage injection from [13

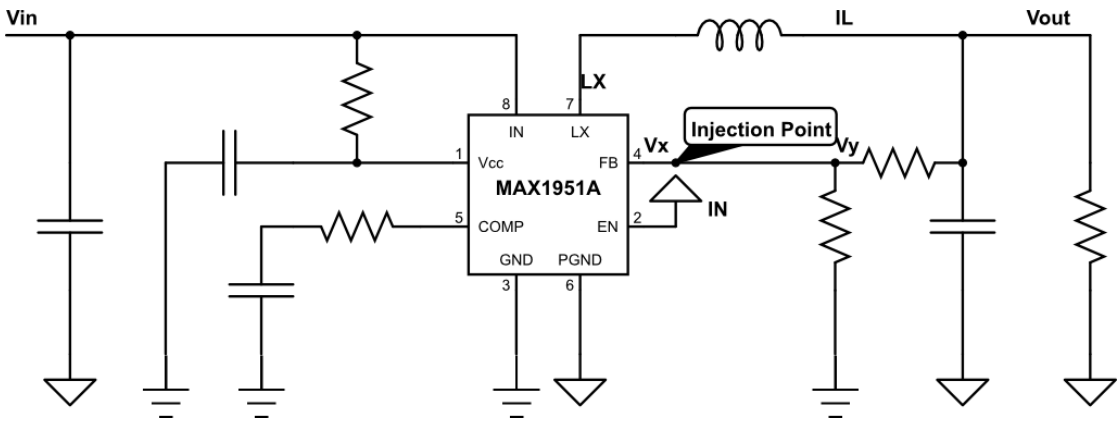

Figure 20. Max1951 measurement locations for Vy, Vx, LX, IL, and Vout

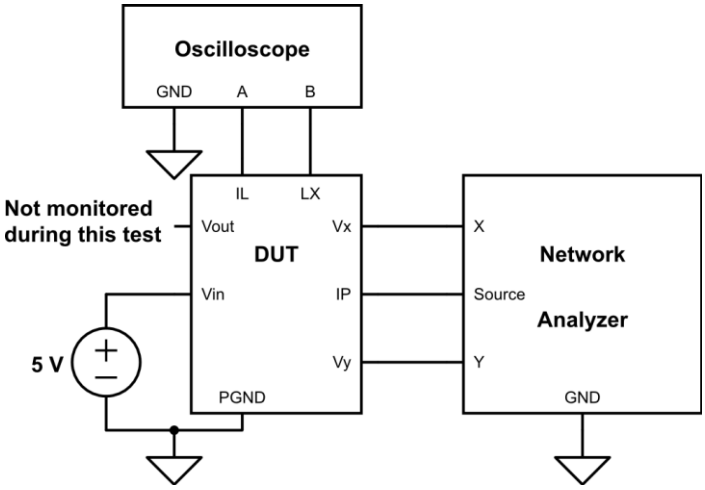

Figure 21. Max1951 measurement setup for loop gain measurement

Monitoring Operating Modes

During the loop gain measurements the Rogowski CWT UM/03/B/1/80 Current Probe was wrapped around the loop of wire connecting to the inductor to monitor the inductor current. A simple voltage probe was also connected to a header at the LX node and ground. The current probe and voltage probe were connected to channel 1 and channel 2, respectively, of a Rigol DS1052E Digital Oscilloscope to check the operating modes of the circuits. A typical operating mode measurement was taken for each dose step characterization, typically around the point of the 2 kHz injection. For circuits that became unstable at injection frequencies with relatively low loop gain, due to loss of the small-signal approximation, an additional measurement or measurements were taken to characterize the instability.

Impedance at the Injection Point Measurement

Prior to irradiation, a measurement of the impedance seen looking into the FB pin was necessary to verify the validity of the injection point of the loop gain measurements. To perform the measurements, only the appropriate BNC connector for the circuit in

question was connected and the same setup was used as to measure the loop gains, with some minor modifications. The Rogowski probe was moved from around the inductor wire to the injection wire and was attached to input R. Then the Network Analyzer was adjusted to measure the magnitude and phase of the voltage probe closest to the Max1951 chip divided by the value of the Rogowski probe. All other Network Analyzer settings remained the same, and the other voltage probes remained in place to keep as similar of a test setup as possible.

Line Regulation

Between each round of radiation and after the loop gain and operating mode measurements, the test board was disconnected from the power supply and connected to two Keithley 2410s. One was connected to the power (Vin) and ground (PGND) banana jacks and was programmed to sweep the DC input voltage from 2 to 5.25 V, with increments of 0.05 V. The other Keithley was programmed to measure an output voltage at each of these increments and was connected to power ground and the output node (Vout) at the load resistor of the circuit under test. Figure 22 shows this test setup for DC characterization. Each circuit was tested individually, with the BNC connector for Circuit A in place first and then subsequently replaced for the BNC connector of each other circuit when it is tested. See Appendix E for the Python code used to perform these measurements.

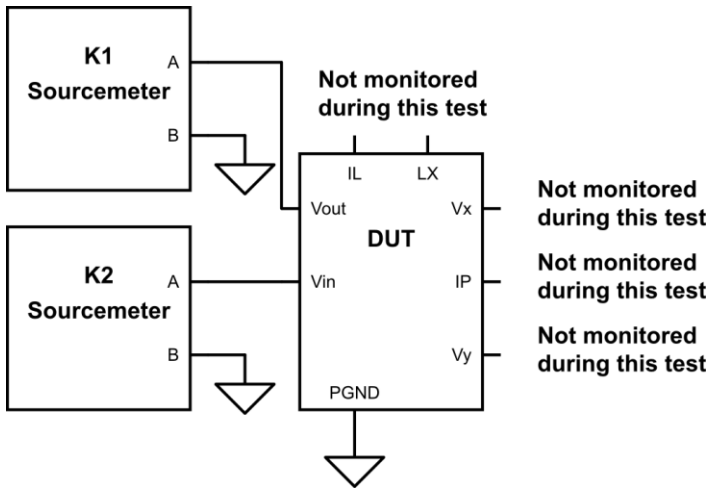

Figure 22. Max1951 measurement setup for DC characterization

CHAPTER V

MAX1951A TEST RESULTS

This chapter provides the results of testing the circuits designed in Chapter III, under the conditions described in Chapter IV. For this chapter, circuits A-C are the three instances of Configuration 1 (nominally 3.3V) and circuits D-F are the three instances that were tested of Configuration 2 (nominally 1.8V). First the results of the impedance measurements are presented to confirm the validity of the loop gain measurements. Then the DC characterization is presented and compared to previous work. Finally, the small signal results are discussed, including a comparison to previous work. Appendix F also includes some additional testing notes.

Impedance at the Injection Point

As discussed in Chapter II, the impedance seen at the injection point is an important factor in determining the quality of loop gain measurement that can be performed, and tends to be more of a problem at higher frequencies [9], [14]. Figure 23 and Figure 24 provide the impedance and corresponding phase, respectively, seen at the injection site. Equipment restrictions of the Tektronix P6022 AC Current Probe mask the information at low frequencies and provide no positive or negative information, but the measurement does confirm the validity of the injection point at high frequencies, i.e., that the forward impedance is high compared to the impedance looking backwards in the direction of signal propagation, over the frequency range of interest.

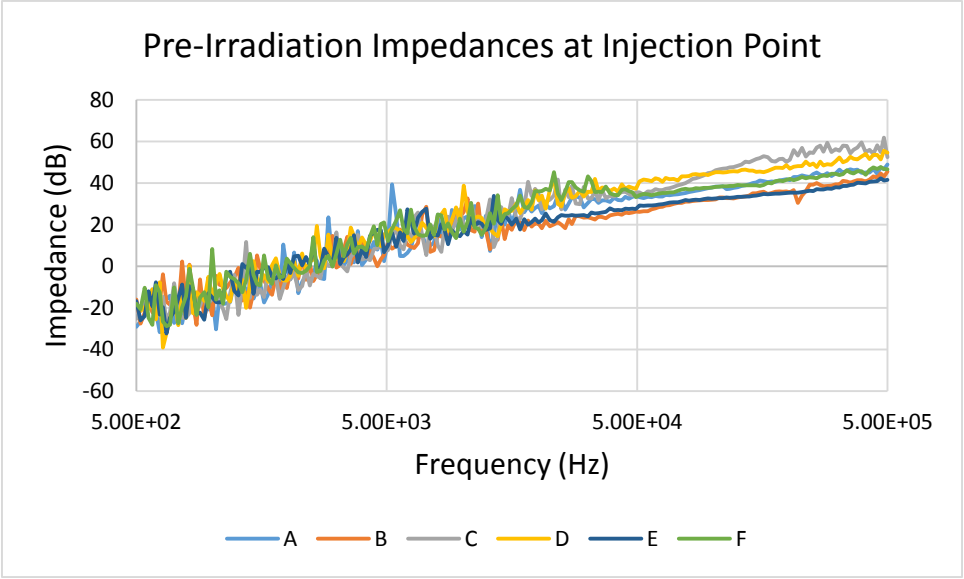

Figure 23. Impedance Verification at the Injection Site for all six Max1951 Converters, pre-irradiation

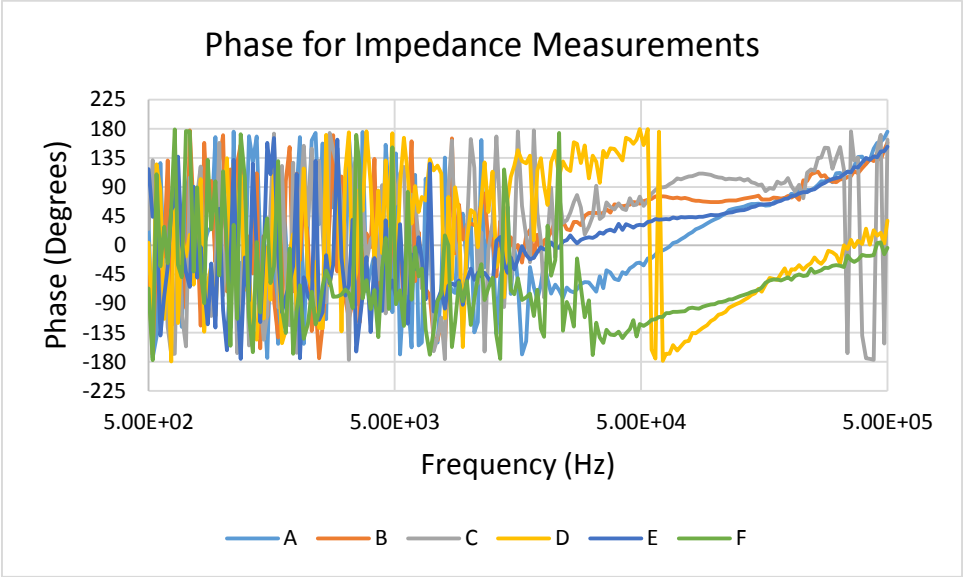

Figure 24. Phase for Impedance Verification for all six Max1951 Converters, pre-irradiation

Large Signal

A DC/DC converter fails when it can no longer create the required output voltage within the datasheet specifications. This section examines the how the DC voltages of the tested MAX1951 converters changed with total dose. Appendix G includes additional DC graphs for completeness.

Output Voltage

The main large signal parameter to analyze is the output voltage. Figure 25 and Figure 26 show some of the DC sweeps for example converters in Configurations 1 and 2, respectively.

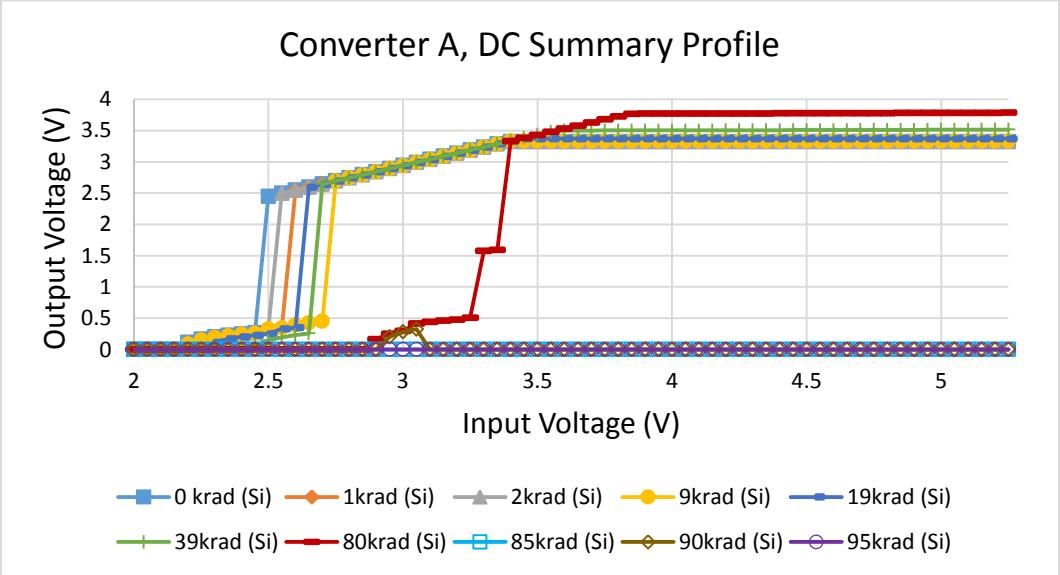

Figure 25. Representative DC sweep for Converters A-C (Configuration 1)

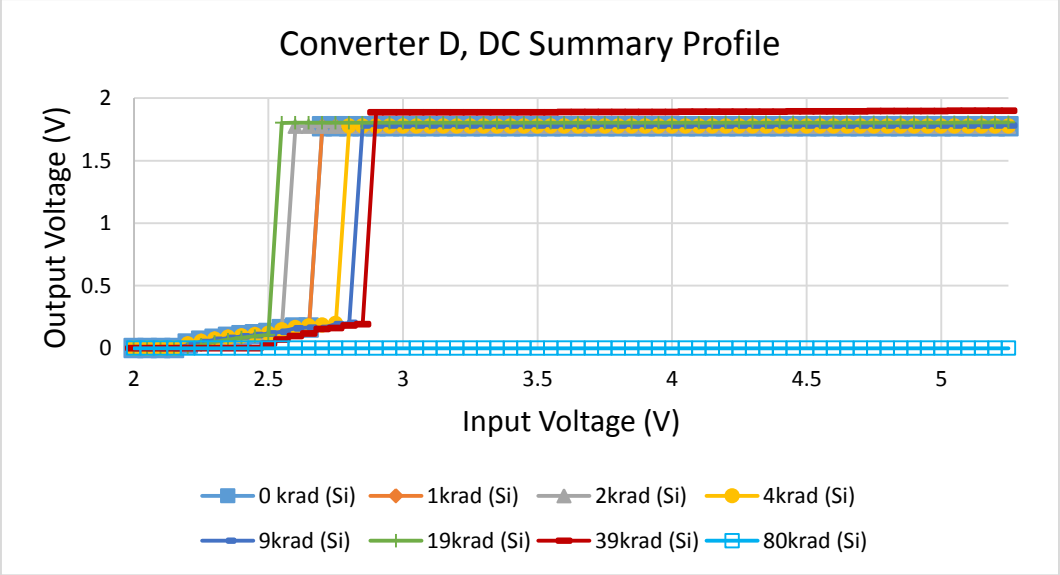

Figure 26. Representative DC sweep for Converters D-F (Configuration 2)

Figure 27 shows the values of the output voltages supplied by the buck converters, when the input voltage was 5V. These output voltages were extracted from the DC sweeps (i.e. in Figure 25 and Figure 26) that were performed on each converter at each dose step.

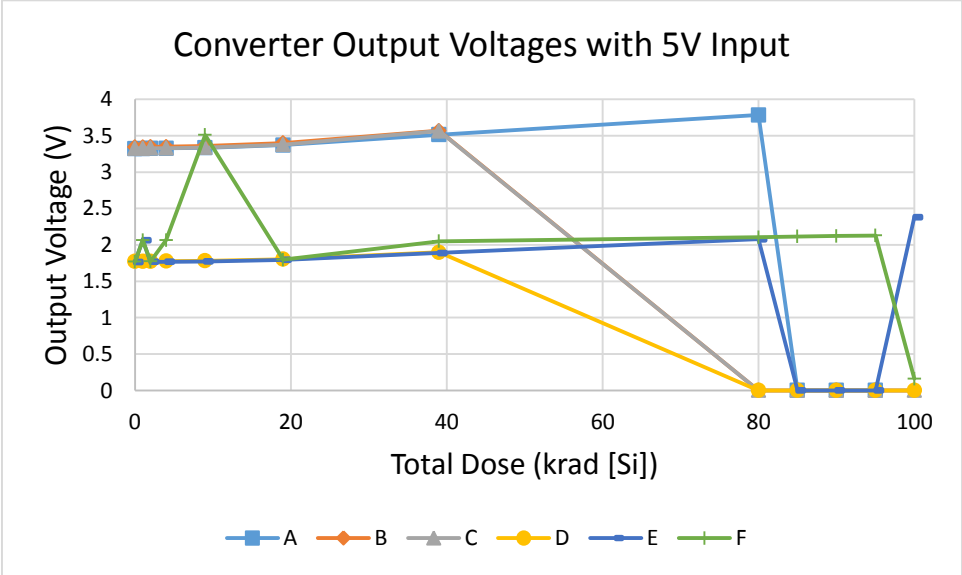

Figure 27. Max1951 output voltages against dose, with 5V at the input

Figure 28 and Figure 29 show the output voltages of buck converters versus TID, from previous work. They show that these switching converters tend to have a fairly steady response, followed by an inability to regulate. Figure 27 suggests that the converters tested for this thesis tended to follow that trend, but further work with smaller dose steps would be necessary to verify this. Figure 30 shows the output voltage versus total dose for four configurations of linear regulator, a different kind of DC/DC converter. This graph suggests that depending on the configuration, linear regulators may or may not experience the sudden cliff-like failure discussed above.

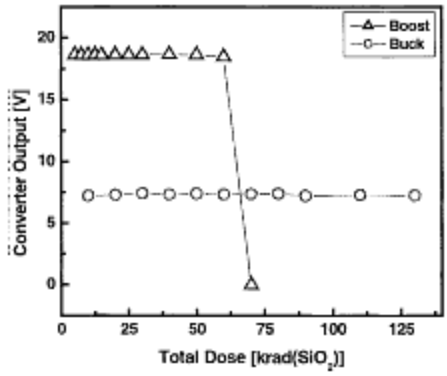

Figure 28. Output voltage vs. total dose for the boost and buck converters, from [8]

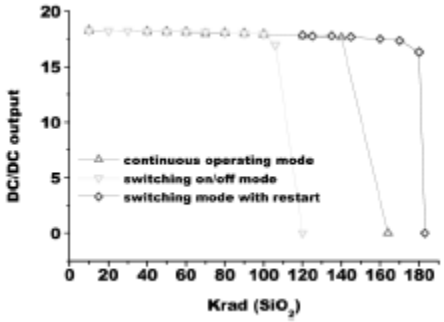

Figure 29. Converter output voltage versus total dose for two methods of characterization described in [9]

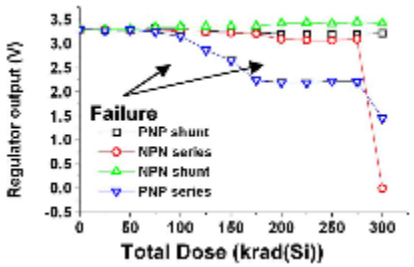

Figure 30. Linear Regulator DC outputs from [10]

Turn-on Voltage

The next large signal parameter that will be discussed is the turn-on voltage. The MAX1951A has built-in circuitry designed to allow the circuit to power up into a pre-biased state at 2.6V [22], so the turn-on voltage is the input voltage where the output voltage is no longer suppressed and goes to this pre-biased state. For the sweeps performed in this test, the step size on the input voltage was large enough that it was clear

where the circuit turned on in most cases. In a few select cases, the built-in circuitry designed to maintain the output at nominally zero volts did not function correctly, so no turn-on voltage was recorded since the circuit did not “turn-on” at a specific voltage. TID could cause this turn-on voltage to shift, depending on the TID response of this control circuitry. Figure 31 and Figure 32 , respectively, show the voltage at which the converters turn on and the output voltage when they turn on after iterative doses of gamma radiation. These figures do not show monotonic changes, which suggests that the changes are not due to radiation, but could be due to thermal variation or other differences between characterizations.

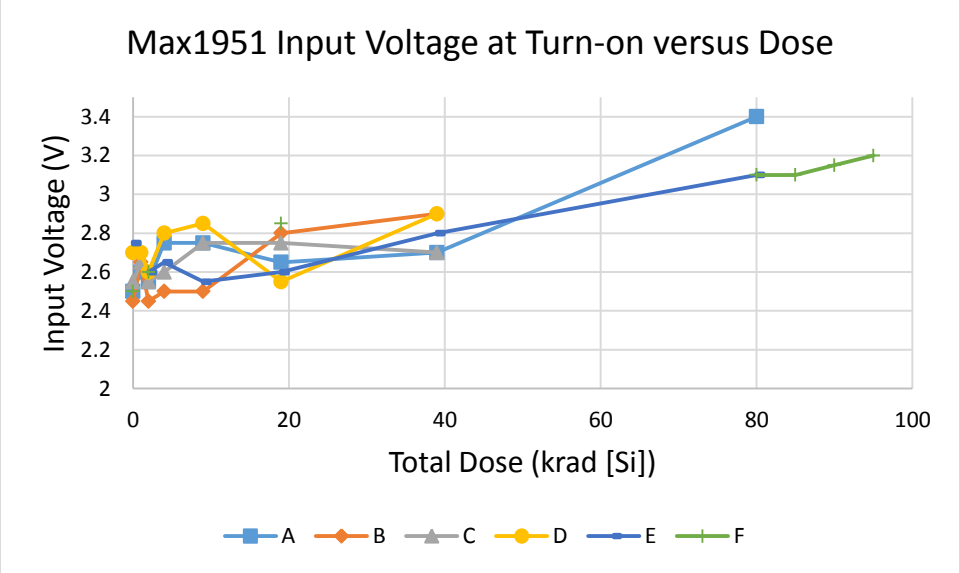

Figure 31. Turn-on Input Voltage

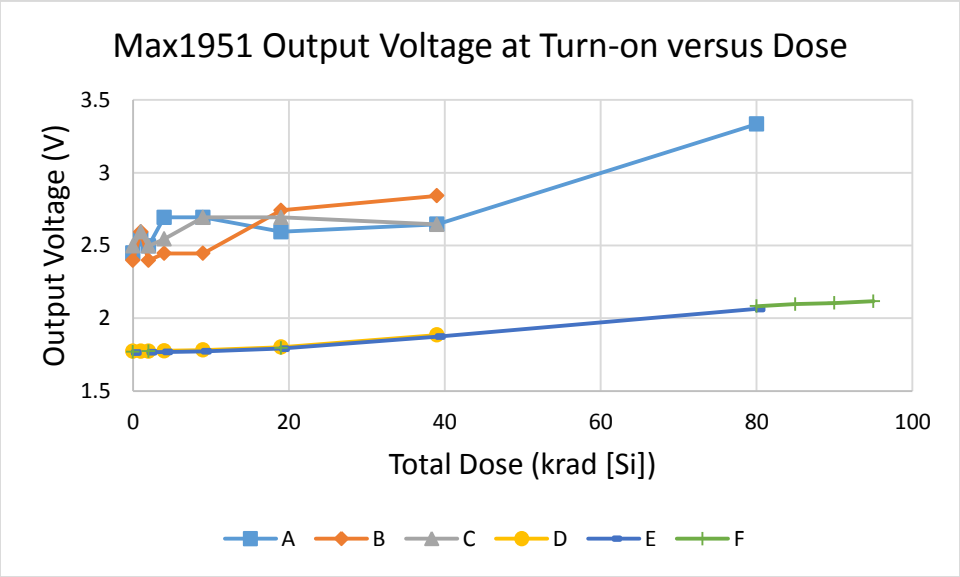

Figure 32. Turn-on Output Voltage

Line Regulation

The final large signal parameter that will be discussed is the line regulation. For the purposes of this thesis, line regulation (LR) is defined as the difference in the maximum and minimum output voltages over the range of interest, divided by the difference in the input voltage over that range, as shown in Equation (39).

$$LR\ (\%) = \frac{V_{out\_max} - V_{out\_min}}{\Delta V_{in}} \times 100\% \tag{39}$$

Figure 33 shows the line regulation over the range that the converter was deemed to be regulating, based on the turn on voltage as the start through the last data point, unless the converter stopped regulating partway through the sweep. In some instances, the converter operated in an improper state during the DC characterization and did not regulate the output voltage. In these cases, a line regulation is not reported for the converter. Figure 34 shows the line regulation over the range that the converter is supposed to operate based on the datasheet's information – after the input reaches 2.6V

or once the input rises above the desired output voltage [22]. In some cases the converter turned on at just over 2.6 V, so this does not provide much information.

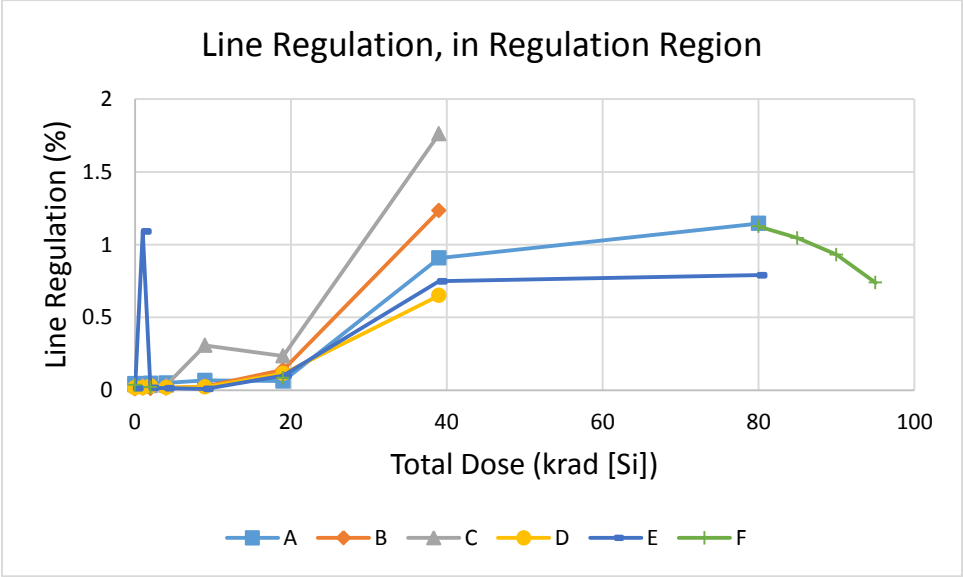

Figure 33. Line regulation in the region of regulation

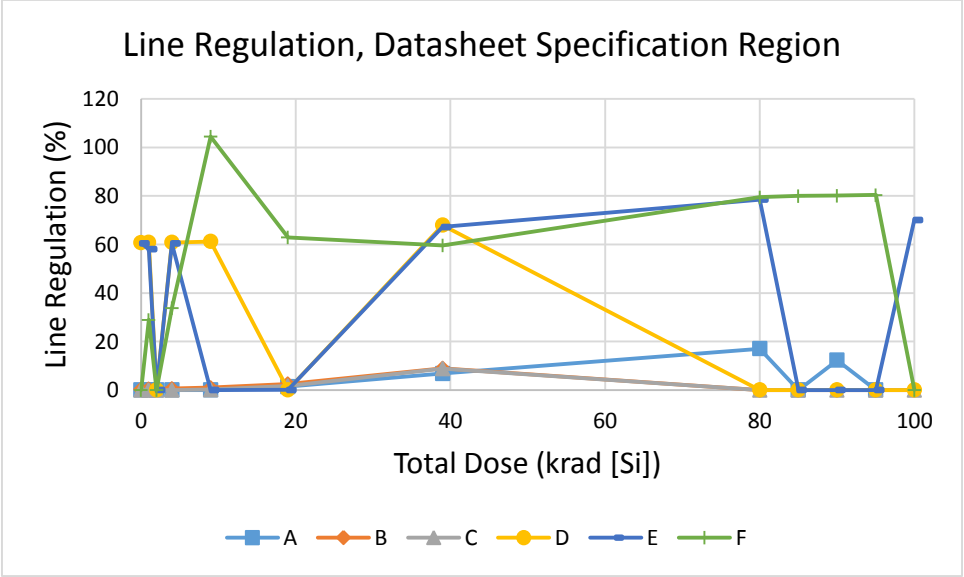

Figure 34. Line regulation in the region of datasheet specification

Small Signal

The small signal data provided in this section is what makes the research for this thesis unique. As shown above, previous work has been done regarding switching

converters and their DC parameters [8], [9]. Previous work has also been done regarding small signal parameters and linear regulators, another type of DC/DC converter [10]. But as known, no work to date has been done regarding small signal parameters and switching converters. This data begins to fill that void.

Loop Gain

As discussed in Chapter II, loop gain is an important parameter for negative feedback systems. In part, it determines how well the feedback system tracks with the desired output. In the case of DC/DC converters, it determines how well the output voltage regulates at a desired voltage, both in terms of how well it tracks with the reference voltage and how well it filters out a disturbance.

Figure 35 - Figure 38 provide the loop gain response of these devices. Figure 35 and Figure 37 demonstrate that the DC/DC converters' inability to create a regulated DC output voltage corresponds to a sudden change in the loop gain. After 85 krad (Si) of total dose, Converter A initially could not regulate and the loop gain had the "failure shape," shown by the curve labeled "85krad (Si)" in Figure 35. However, after a power cycle, the circuit returned to operation and the loop gain returned to the same general shape of previous measurements. This loop gain curve is labeled "85Bkrad (Si)" in Figure 35. After 90 krad (Si), Converter A went into the failure mode and did not return to an operative state. After 80 krad (Si), Converter D went into a permanent failure state. Closer examination of the loop gain data, shown in Figure 36 and Figure 38, reveals that the small change in the output voltage prior to total failure corresponds to an incremental shift to the right of the loop gain curve, with increasing total dose.

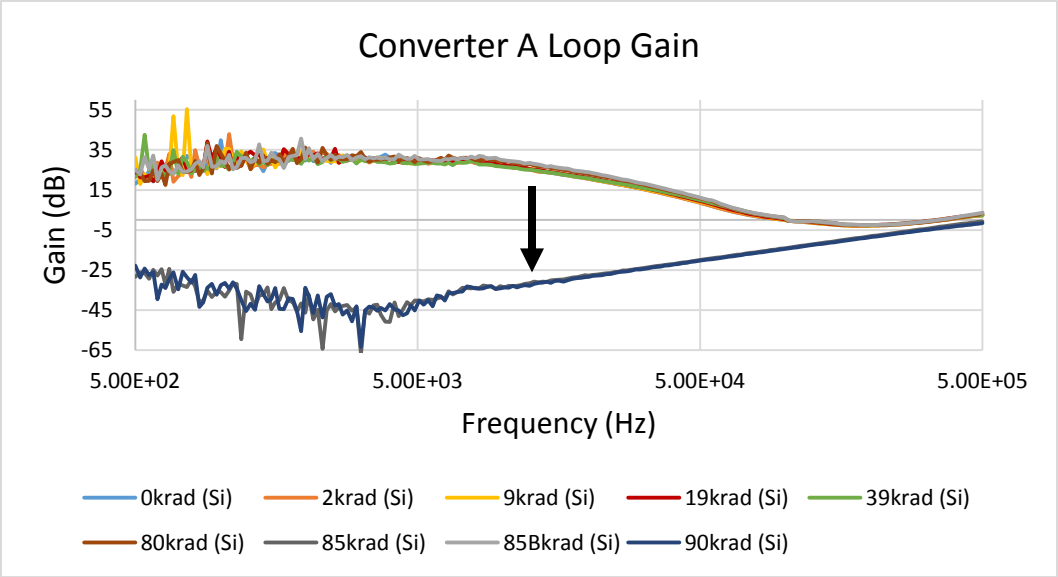

Figure 35. Converter A, from Configuration 1, loop gain at different total doses

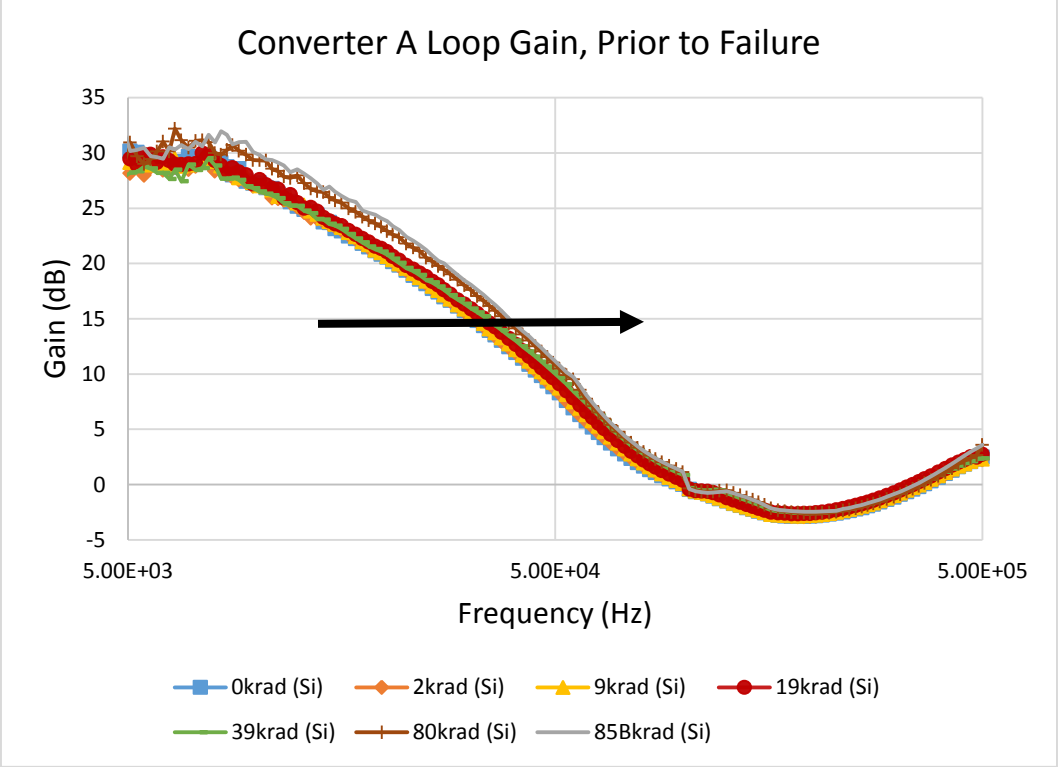

Figure 36. Converter A, from Configuration 1, loop gain at different total doses, prior to failure

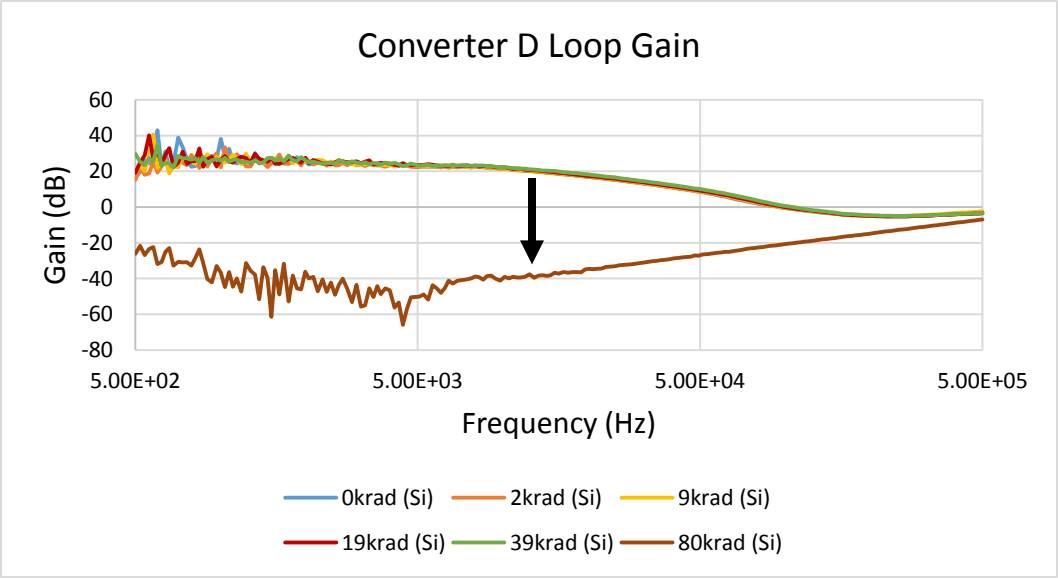

Figure 37. Converter D, from Configuration 2, loop gain at different total doses

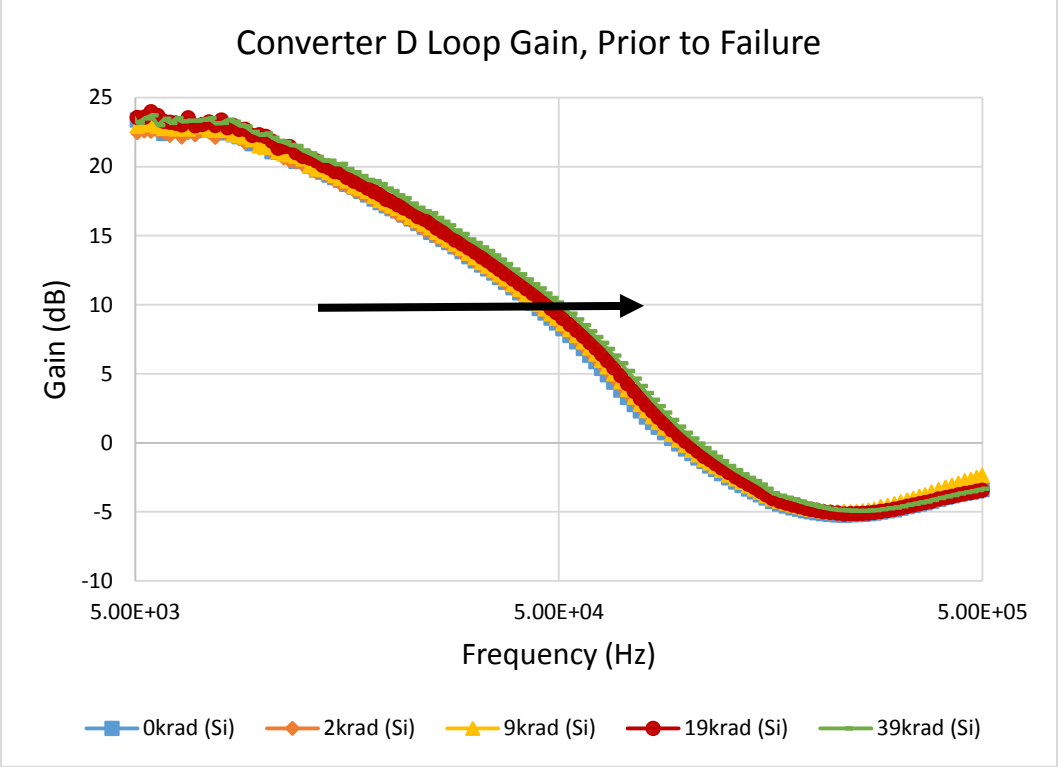

Figure 38. Converter D, from Configuration 2, loop gain at different total doses, prior to failure

This data is in partial agreement with Kelly's work on linear regulators [10], as mentioned in Chapter II. Similar to Kelly's results, the loop gains of these converters experienced an incremental shift with total dose. Additionally, some of Kelly's

configurations showed a sudden change in the shape of the loop gain at relatively high doses. The loop gain of the buck converters tested for this thesis also experienced a sudden shape change at high doses. These similarities suggest that the most sensitive component to TID within buck converters is also the error amplifier, but further testing would be necessary to verify this assessment. However, the data presented here dose have some differences from Kelly's work. Unlike the loop gain curves in Kelly's work which degraded down/to the left with increasing dose, the loop gain curves presented here shifted up/to the right with increasing dose. One possible explanation for this difference is the different bias points of the error amplifiers. Previous work [18] has shown that threshold shifts due to ionizing radiation on power MOSFETs are bias dependent, including whether or not the bias is switching or constant. This could explain the different direction of shift. Further information on the internal circuitry of the Max1951 as well as further testing would be necessary to explore this difference.

Phase

The phase of the buck converters was also recorded during loop gain measurements. Figure 39 and Figure 41 show the general shape of the phase that corresponded with the loop gain measurements for Configuration 1 and Configuration 2, respectively. The significant variation at lower frequencies is believed to be due to equipment limitations at low frequencies, most likely from the current probe that was used to inject the signals into the circuit. Figure 40 and Figure 42 provide a better view of the point where the phase reaches 180 degrees. This data was used to examine information regarding the stability of the circuit through measures such as crossover frequency, phase margin, and gain margin. Figure 43 provides the gain margin – the gain

magnitude when the phase goes to 180 degrees – information derived from the phase and loop gain measurements. The other two metrics are included in Appendix H. Other than one measurement performed on Converter B when it was in an unusual operating mode, the gain margins shown in Figure 43 are all negative in dB, which means that the converters should be stable. The stability concerns are addressed further in the following section.

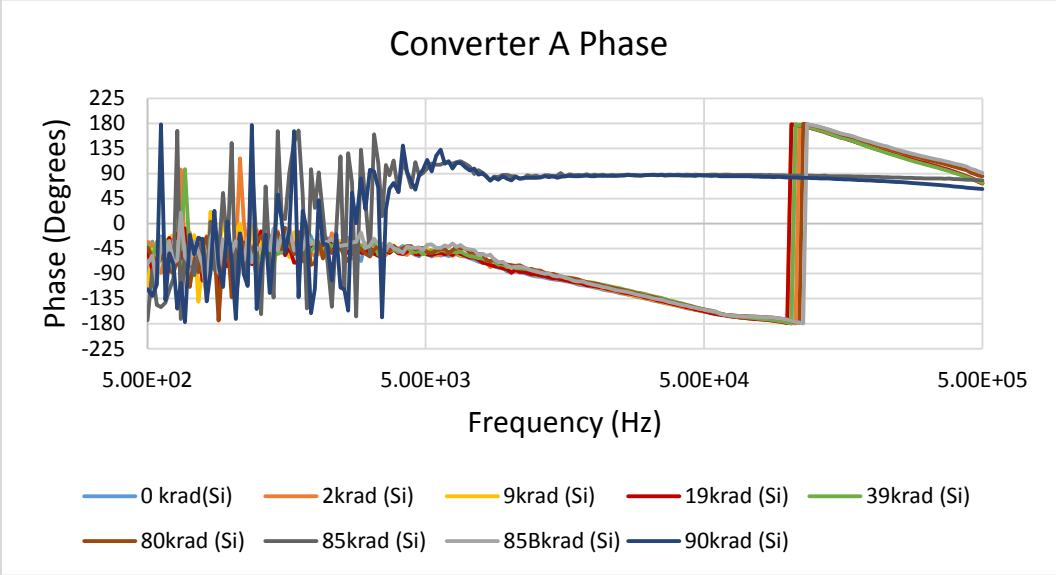

Figure 39. Converter A, from Configuration 1, phase at different total doses

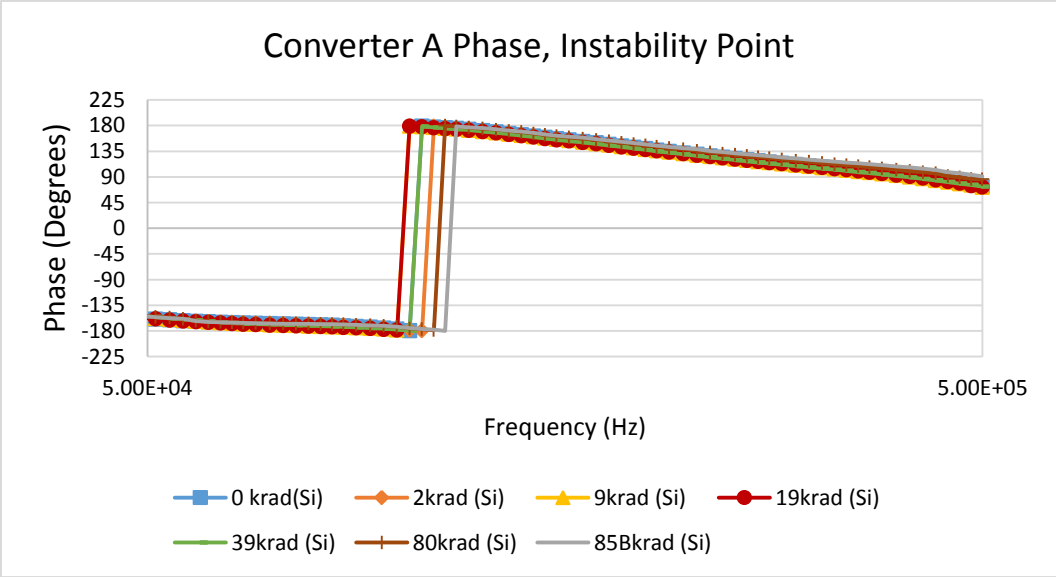

Figure 40. Converter A, from Configuration 1, phase at different total doses, around the point of instability

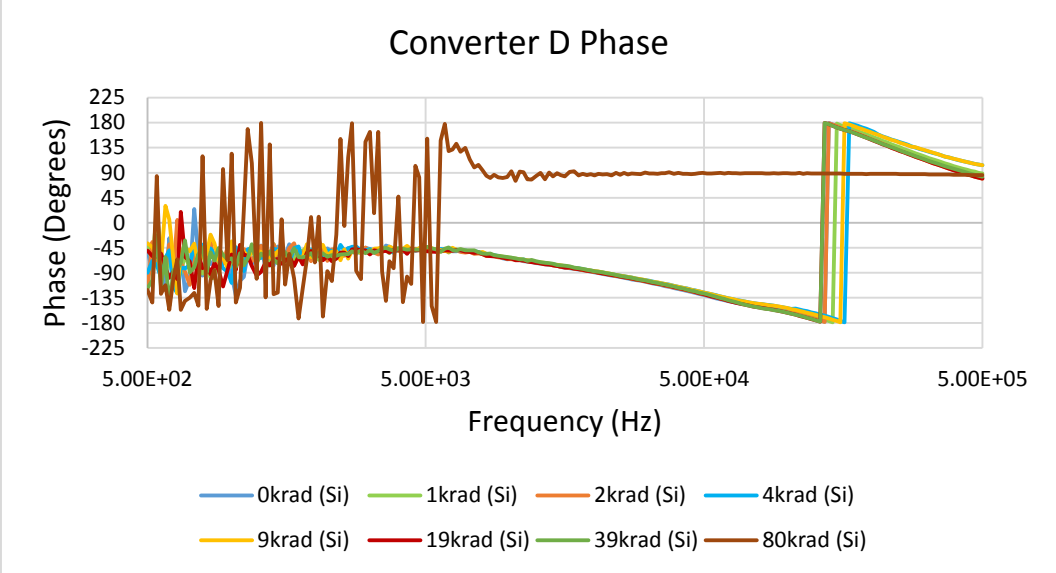

Figure 41. Converter D, from Configuration 2, phase at different total doses

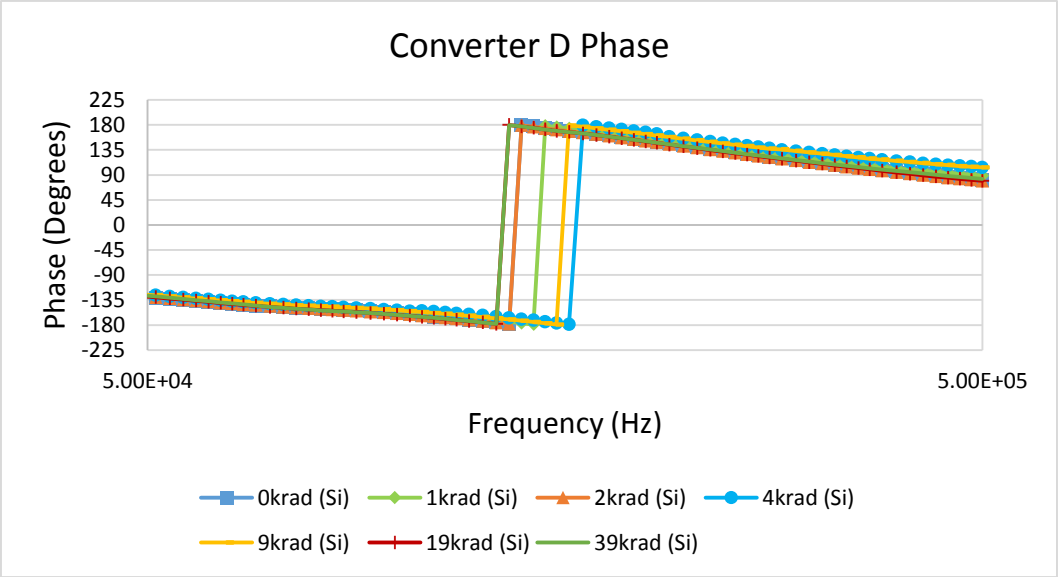

Figure 42. Converter D, from Configuration 2, phase at different total doses, around the point of instability

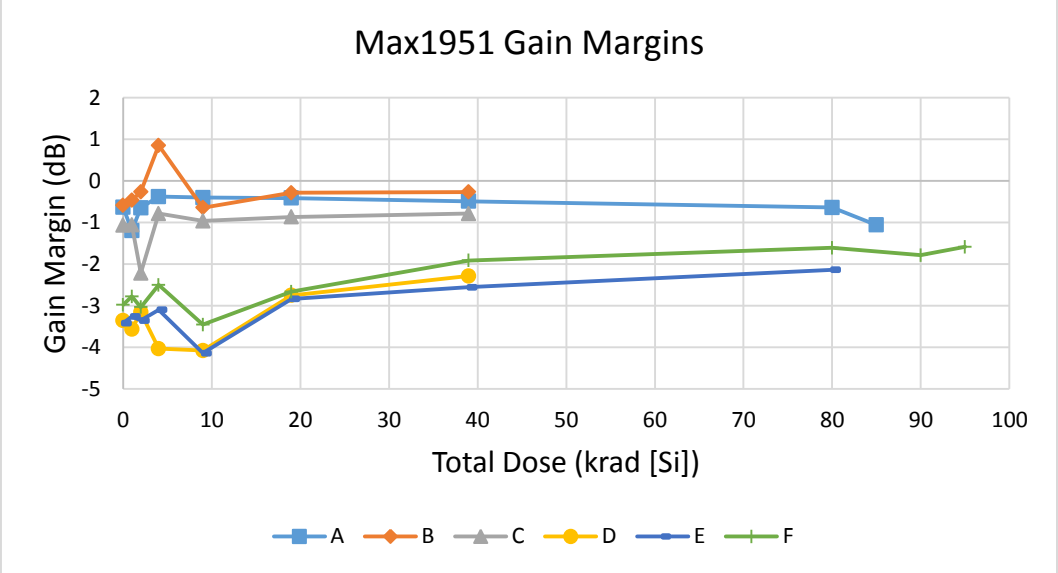

Figure 43. Gain margins for tested Max1951A converters

Operating Mode Information

In order to verify that the small signal loop gain measurements were in the correct operating mode and were valid, the inductor current and voltage at the LX pin of the device under test were observed during loop gain characterization. This observation showed that throughout most of each loop gain measurement, the converters performed

as expected, with the inductor current ramping up and down as the LX point switches on and off, as seen in Figure 44 and Figure 45. The values of the inductor current and LX voltage have been scaled to show that they correspond with each other, similar to how they were monitored on the oscilloscope during testing. The specific values of these quantities are unimportant. As a note, the length of the LX on time, t_{on}, is longer for Configuration 1 than it is for Configuration 2 because Configuration 1 is designed for the higher output voltage, which corresponds to a larger duty cycle – see Equation (1). As the loop gain becomes small and nears its crossover frequency, the perturbations of the injected signal from the network analyzer no longer follow the requirements of a small signal approximation. Instead, the injected signal adjusts the bias point of the circuit, which is seen by a lower frequency envelope in addition to the switching frequency. This was observed on the oscilloscope during operation and can be seen in Figure 47. The claim that instability is caused by violation of the small-signal approximation rather than by changes in the circuits due to total dose is supported by the negative gain margins for the circuits, previously shown in Figure 43.

As shown in Figure 46 and Figure 47, the Configuration 1 circuits experienced a greater change in inductor current than the Configuration 2 circuits. This shows that the initial circuit design for Configuration 2 was more stable than the initial circuit design for Configuration 1. This is further shown by the fact that the switching of the LX voltages changed much more significantly during this injection for Configuration 1 than it did for Configuration 2, as seen in Figure 48 and Figure 49. The output voltage of a buck converter is directly related to the input voltage and the duty cycle, as seen in Equation (1). Figure 48 shows the LX voltage during the loop gain measurement. The value of the

duty cycle was different when the loop gain approached the cross-over frequency from when the converter was in stable operation. This shows that the converter's output voltage varied throughout the injection, particularly at the point of instability near the loop gain's cross-over frequency. The small-signal approximation is no longer valid when the injection signal causes the DC output voltage to fluctuate. A change in the mode of operation such as this causes a change in the loop gain. Figure 36, re-shown below with slight modification as Figure 50, shows a change in the general shape of the loop gain near the crossover frequency (within the circle). The change of the shape of the loop gain is likely due to this change in the mode of operation. Converter B and Converter C were even more prone to mode changes than Converter A. To see those loop gain measurements, and the sudden changes that mark mode of operation changes, see Appendix H. Visual confirmation during measurement revealed that these deviations from smooth loop gain curves do correlate to changes in the inductor current and LX voltage, as seen on the oscilloscope.

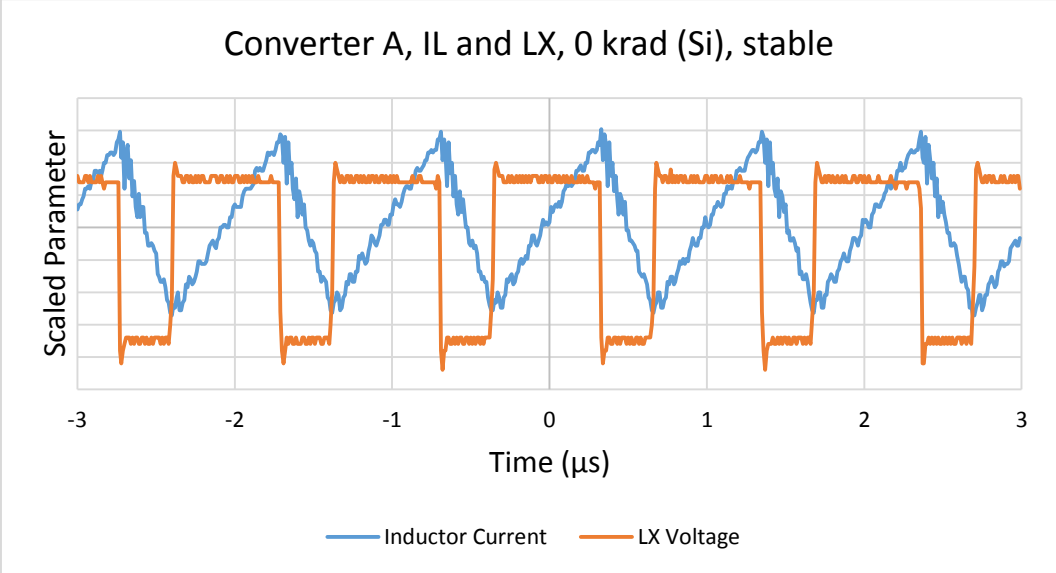

Figure 44. Typical IL and LX during loop gain measurement, Configuration 1

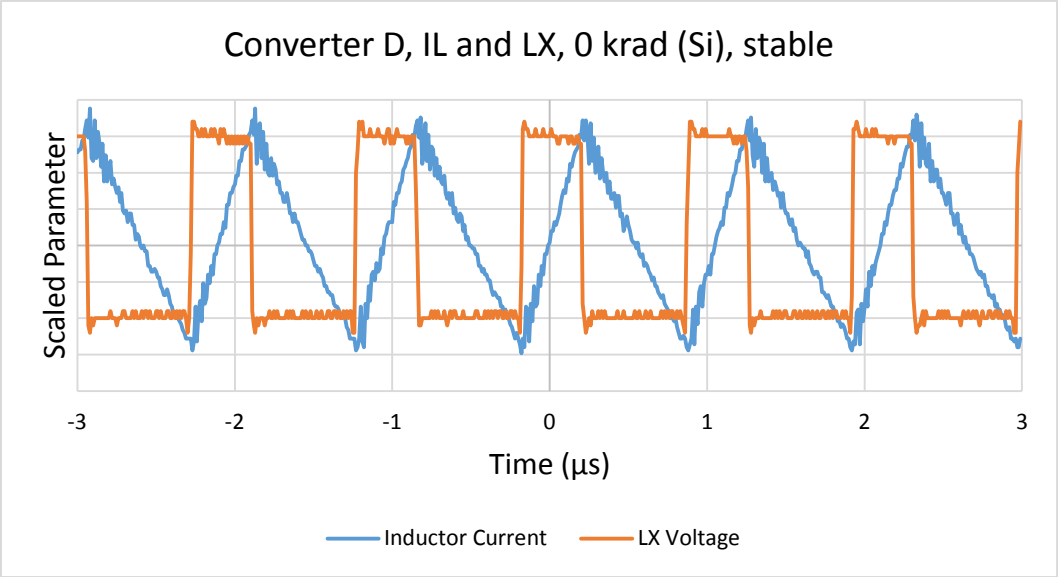

Figure 45. Typical IL and LX during loop gain measurement, Configuration 2

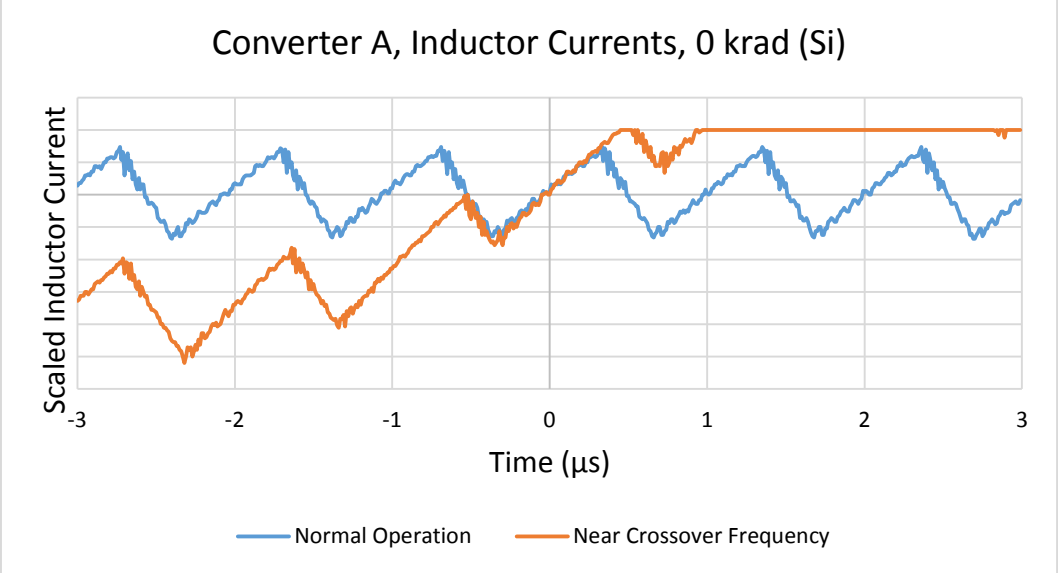

Figure 46. Inductor currents during loop gain measurement, Configuration 1

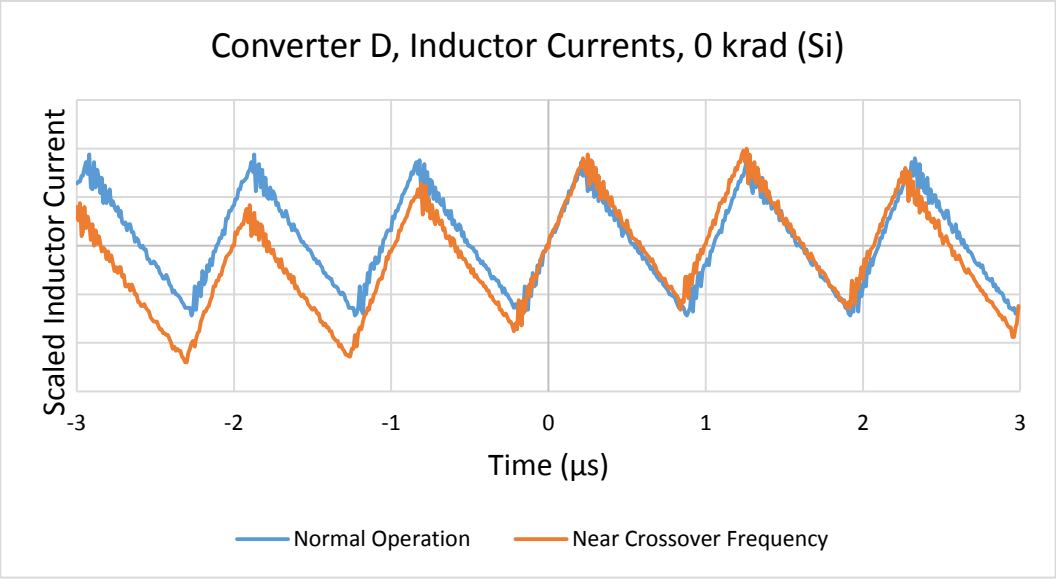

Figure 47. Inductor currents during loop gain measurement, Configuration 2

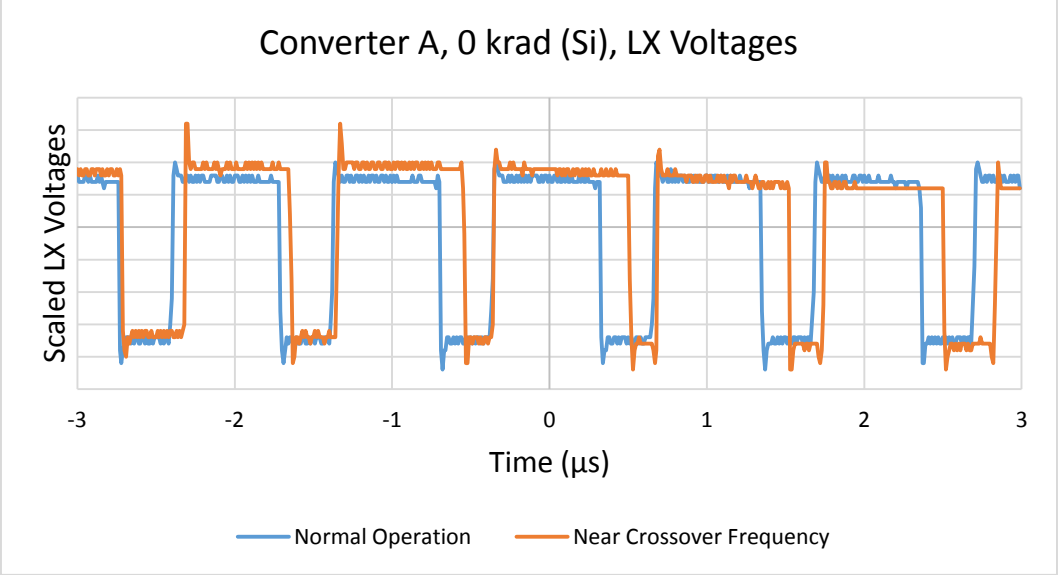

Figure 48. LX voltages during loop gain measurement, Configuration 1

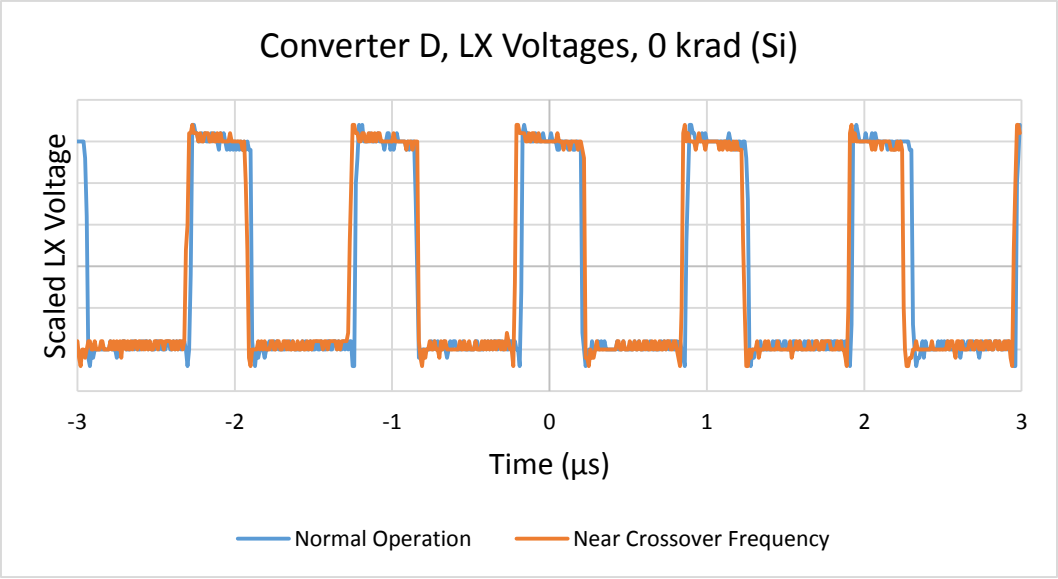

Figure 49. LX voltages during loop gain measurement, Configuration 2

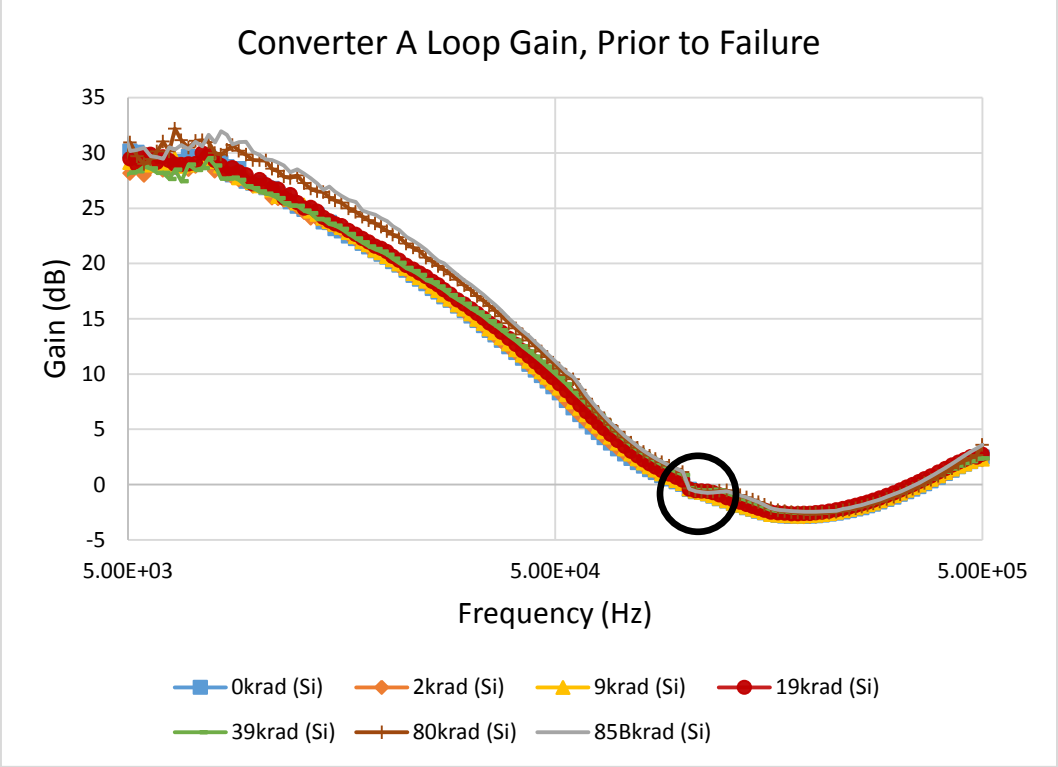

Figure 50. Converter A, from Configuration 1, loop gain at different total doses, prior to failure

CHAPTER VI

CONCLUSIONS

This thesis examined the effects of TID on an integrated COTS buck converter's ability to regulate the output voltage and the corresponding changes in small signal parameters. The inclusion of small signal parameters for this experiment as well as the analysis of an integrated converter are new for the radiation effects community and suggest further areas of research. Two circuit configurations of the Max1951 were examined to compare how differences in the biasing conditions could change the radiation response of the loop gains. One configuration experienced stability concerns due to the measurement technique, but the loop gain trends in both configurations were consistent.

The DC characterization of the buck converters was shown to be fairly consistent with previous research that has been done regarding switching converters and their responses to TID. Small changes in the output voltage, in this case small increases, correlated with increasing total dose. Additionally, there was a point of clear failure where the output voltage decreased significantly from previous measurements. This thesis also explored potential changes in the supervisory undervoltage lockout circuitry. However, no trends were identified regarding this control circuitry.

The analysis of small signal parameters against total dose provided the most interesting information. The loop gain and crossover frequency increased with increasing total dose, followed by a significant decrease of loop gain at the point of failure. These shifts correlated with the shifts in the DC voltage, and the decrease coincided with the converters' inability to regulate the output voltage. These results are similar to previous

work done by Kelly on linear regulators, which suggest that the error amplifier or transconductance amplifier, as seen in the block diagram of Figure 14, may the most sensitive component(s) within the buck converter. Equation (40) is Equation (2) without the disturbance e(s) and applied at the DC frequency of 0 Hz. It shows that increases in the loop gain T(s) should cause the output voltage to more appropriately track with the ratio of the reference voltage and the DC feedback gain, H(0). If the loop gain were decreasing at the DC point, then the output voltage should be decreasing correspondingly. Since the loop gain of the tested converters changed and the DC output voltage increased with increasing total dose, another mechanism is likely involved. The most likely mechanism for these changes is a change in the offset voltage of either the error amplifier or transconductance amplifier. Since these components are in the loop gain path, their TID response could cause an increase in the output voltage. This further supports the claim that these may be the most TID sensitive components within the tested converter.

$$v_{out} = \frac{1}{H(0)} \frac{T(0)}{1+T(0)} v_{ref} \tag{40}$$

This information provides opportunities for future research. The undervoltage lockout circuitry did not demonstrate any clear trends, but this supervisory circuitry is commonly included in integrated switching converters so it could be the focus of additional research. Additionally, the COTS POL converter tested in this experiment was surprisingly radiation tolerant for moderate TID dose, as the loop gain and output voltage experienced moderate changes, but was prone to complete failure at a dose of tens of krad (Si) at which point regulation was lost. Further work to understand this failure mechanism could prove valuable for understanding the sensitivity of switching converters to total ionizing dose.

APPENDICES

The following appendices provide supplementary material concerning the experimental design and data presented in the main body of the thesis.

Inductor Design

The application note [22] suggests using a 2 μH so this was followed for the tests performed in this thesis. However, the calculations provided in the application note suggest that a significantly different value should be used and even says to "not use output inductors larger than 2.2 μH" [22]. Future testing may consider using a different sized inductor though. Those calculations are shown below.

$$L_{Init} = V_{Out} \frac{V_{In} - V_{Out}}{V_{in} \times LIR \times I_{Out\ (MAX\ )} \times f_{sw}} \tag{41}$$

Equation (41) from [22] is used to calculate a reasonable inductor value that can then be rounded to commonly available values. V_{Out} is the output voltage of the circuit configuration and V_{In} is the input voltage which is assumed to be 5 V for calculations, since this is the voltage used for irradiation and during loop gain measurement. LIR is the inductor current ripple percentage and should be kept between 20% and 40% [22], so it is assumed to be in the middle at 30% for calculations. $I_{Out(MAX)}$ is the load current, which is known for each configuration and f_{sw} is the switching frequency of the oscillator which is typically 1 MHz [22]. In Equation (42), $I_{Out(MAX)}$ has been replaced with V_{Out} divided by R_{Load}, the output voltage divided by the load resistance which is equivalent to the output current by Ohm's Law. Equations (43) and (44) have the values for Configuration 1 and Configuration 2, respectively, substituted into Equation (42)

$$L_{Init} = V_{Out} \frac{V_{In} - V_{Out}}{V_{in} \times LIR \times \frac{V_{Out}}{R_{Load}} \times f_{sw}} \tag{42}$$

$$L_{Init} = 3.4V \frac{5V-3.4V}{5V \times 0.3 \times \frac{3.4V}{18\Omega} \times 10^6 Hz} = 19.2\ \mu H \quad (43)$$

$$L_{Init} = 1.8V \frac{5V-1.8V}{5V \times 0.3 \times \frac{1.8V}{5\Omega} \times 10^6 Hz} = 10.7\ \mu H \quad (44)$$

In both cases, the calculated values for inductor size are significantly larger than those suggested by the application note (and therefore used in the test). Future testing should consider using larger inductor values.

Construction

This appendix provides a little more information about the construction of the circuits that were tested for this thesis. Initially a pathfinder prototype was built on a circuit board that did not have a ground plane and then was tested. Care was taken to minimize the lengths of wire traces and parasitics. The circuits tested for the data in this thesis were all built on the same circuit board, but it did have a ground plane. The chosen circuit board was an 8004 perforated prototype board from vector electronics. The wire connections were changed slightly to take advantage of the ground plane, so one test circuit was built before the others to ensure correct operation, as shown in Figure 51, after this the remaining five circuits were built simultaneously in assembly-line fashion. Figure 52 - Figure 58 show the construction of these circuits, with the explanation of each step in the captions. The components listed refer to the names in Figure 10 and Figure 9.

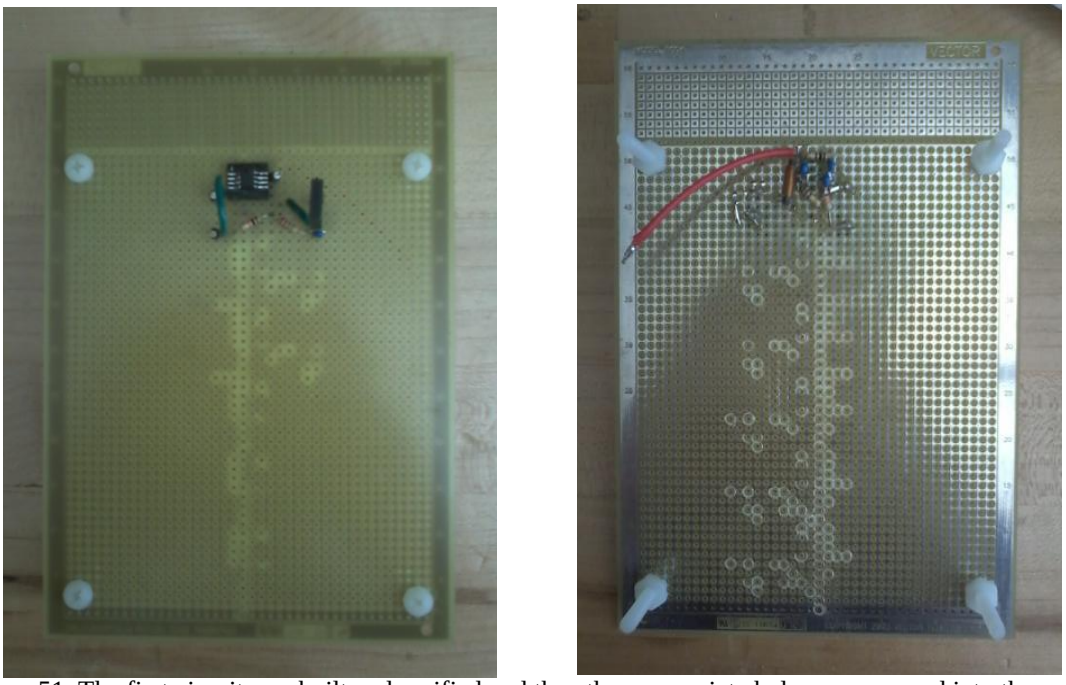

Figure 51. The first circuit was built and verified and then the appropriate holes were carved into the ground plane for the other circuits

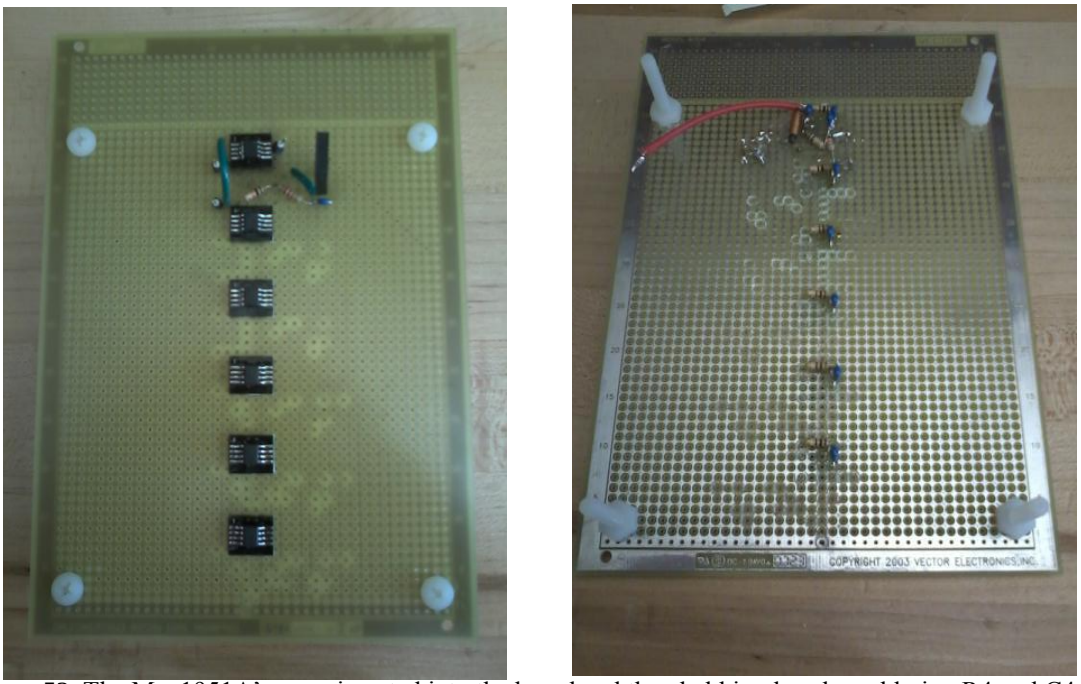

Figure 52. The Max1951A's were inserted into the board and then held in place by soldering R4 and C4

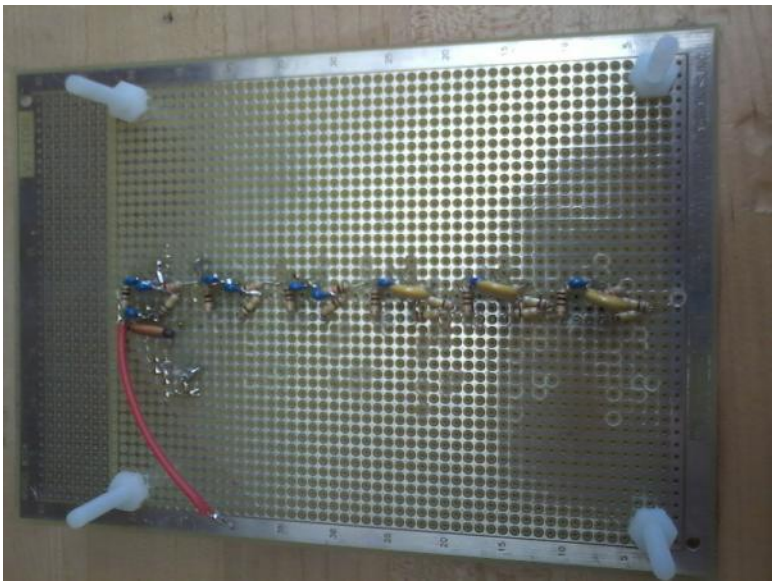

Figure 53. Next R1 and C2, the compensation resistor and capacitor, were put in place

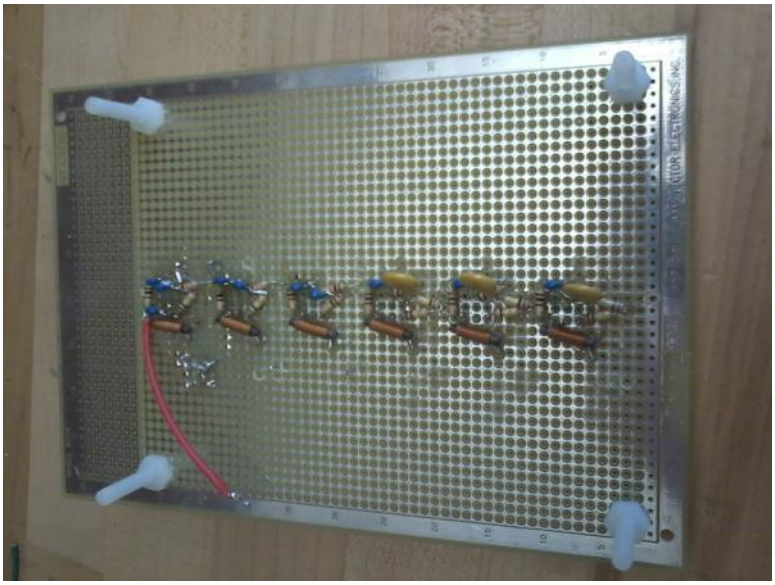

Figure 54. Next L1, the inductor, was put in place

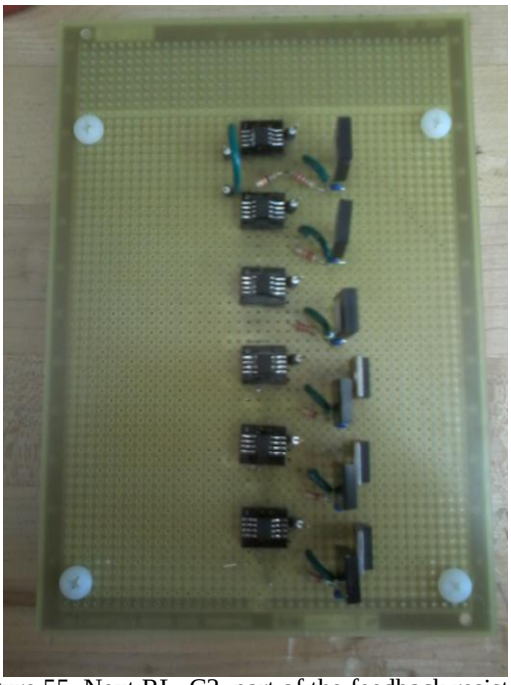
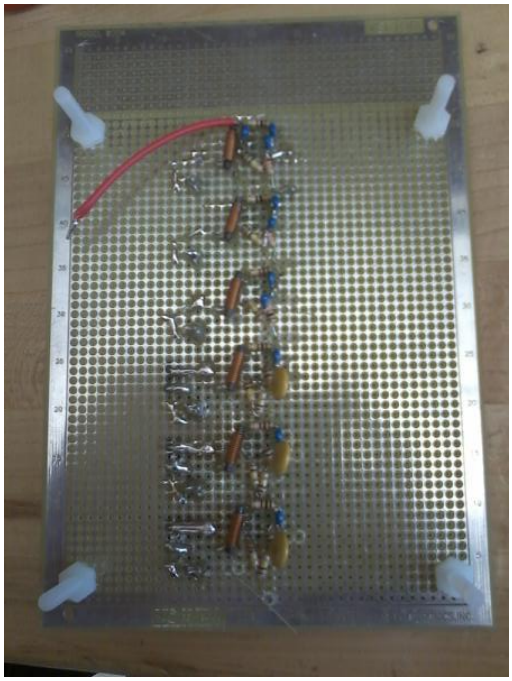

Figure 55. Next RL, C3, part of the feedback resistor network, the LX voltage probe point, and the inductor current monitor wire were put in place

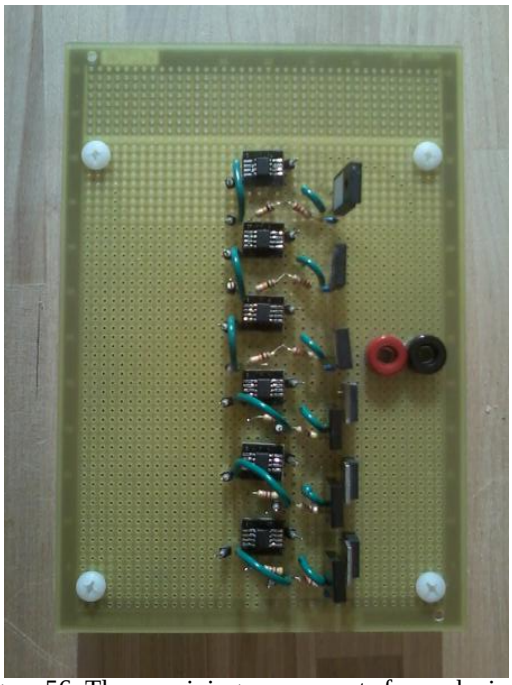
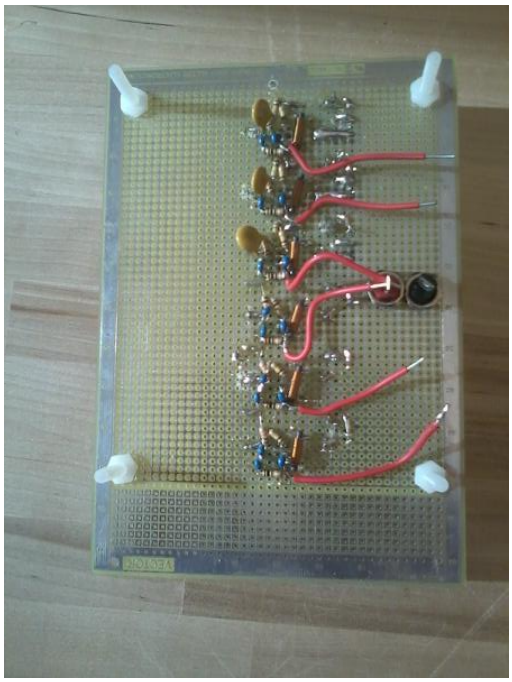

Figure 56. The remaining components for each circuit were put in place and the banana jacks were added. Then the circuits were tested to ensure that having multiple converters on one power line would not cause inappropriate operation

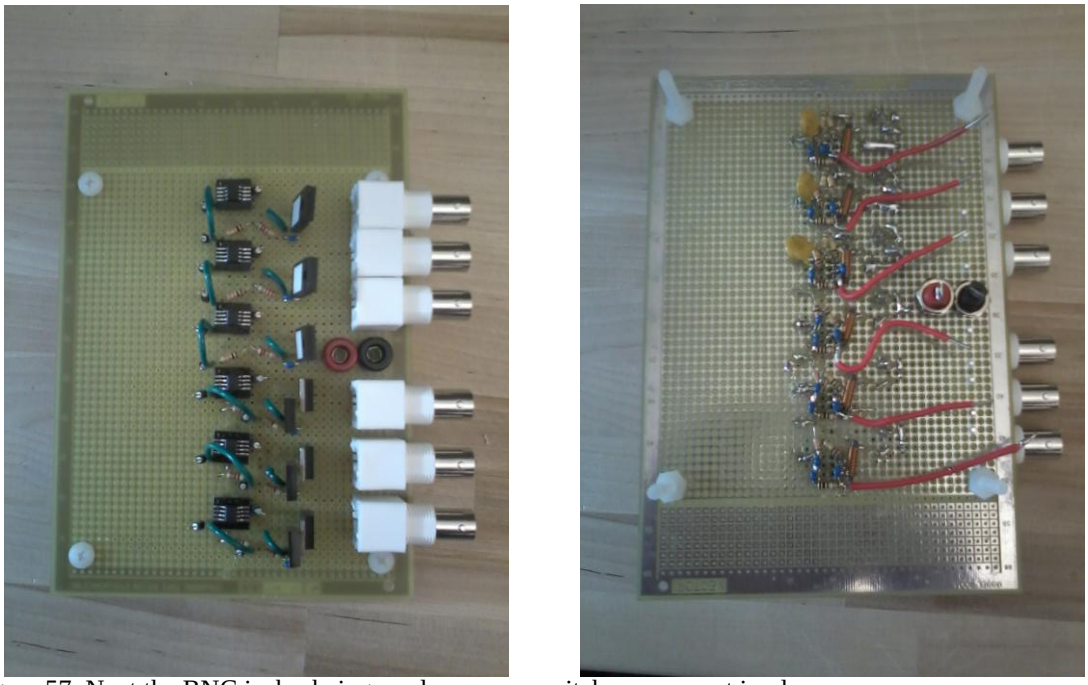

Figure 57. Next the BNC jacks, being used as power switches, were put in place

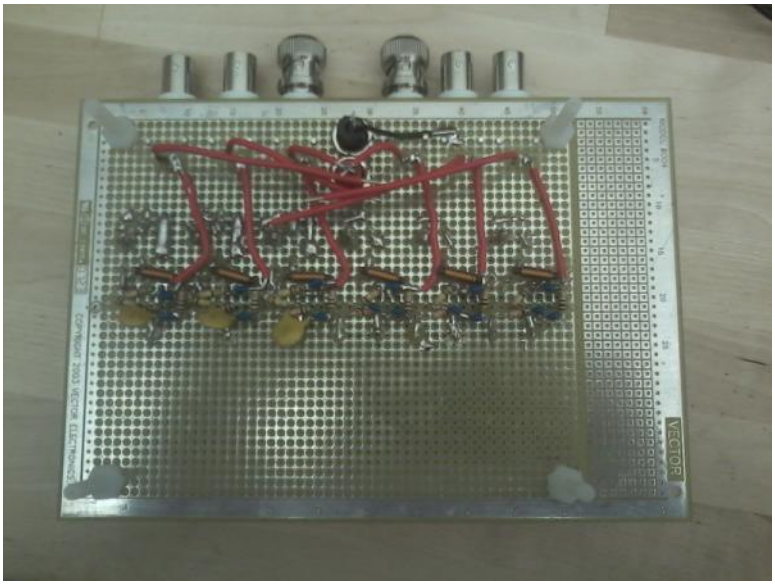

Figure 58. Finally, the power wires were soldered from the circuits to the BNC jacks and from the BNC jacks to the banana jacks

Half-life Calculator

This section explains how the dose rates, and therefore total doses, were determined. There is an excel document which has information characterizing the dose rates at different distances from the Sheppard Cell Cs-137 source. This document also has

a calculator to determine the dose rates at given distances for a given date, based on known half-life information. The dose rates for June 2, 2014, the date of the tests, are shown in Table 3. 12.5 cm from the source was selected from this list and then the corresponding dose rate was used to calculate the total doses experienced by the tested circuits.

Table 3. TID dose rate information for the Cs-137 source on June 2, 2014

From Mike Freeman measured 01/18/12 Dose rate Gy/min	measured 01/18/12 Dose rate rad(Si)/min	corrected to 06/02/14 Dose rate rad(Si)/min	Distance, cm
25.29	2529.0	2394.4	0
10.85	1085.0	1027.2	2.5
6.86	686.0	649.5	5
2.99	299.0	283.1	12.5
1.81	181.0	171.4	20.5
1.21	121.0	114.6	28
0.96	96.0	90.9	33

MATLAB Code

After the pathfinder test determined that these circuits may fail around 80 krad (Si), a simple MATLAB formula (shown below) was used to calculate logarithmic spacing of the dose steps. This allows for trends to be identified more easily and then smaller dose steps of 5 krad (Si) were taken to determine the point of failure for the circuits that had not failed by 80 krad (Si). These doses are seen in Table 2.

```
>> Drounded = round( logspace(log10(1),log10(80),7) )

Drounded =

   1    2    4    9   19   39   80
```

Python Code

The following code was supplied by Colin Thomas and was used to perform the DC sweeps, as described in Chapter III in the Line Regulation section. The code is supplied here for future researchers to be able to more easily emulate the tests.

```
from data import k2410
from data.colin import *
import msvcrt, time, datetime, numpy, getopt, os, sys


addr = '169.254.58.10'
data_file="%s_%s_linReg.csv"
dev0 = ['k_bias',0.35,0.05,'1.']
compliance = 0.005 #amps
test_voltages1951 = numpy.arange(2, 5.3, .05)
test_voltages750 = numpy.arange(3.5,10.6,.1)


def M1951(rad_level, fuse_num):
        set_v(k1,0,compliance)
        fid = open(data_file % (fuse_num, rad_level), "w")
        fid.write("leakage current for fuse %s at dose %s\n"%(fuse_num, rad_level))
        fid.write("volt1,curr1,volt2,curr2\n")
        set_c(k2,0,compliance) #measure voltage by sourcing 0 amps
        on(k1)
        on(k2)
```

```
for voltage in test_voltages1951:
        set_v(k1,voltage,compliance)
        [v1,c1] = get_vi(k1)
        [v2,c2] = get_vi(k2)
        fid.write('%0.16f,%0.16f,%0.16f,%0.16f\n'%(v1,c1,v2,c2))
        print v1, c1,v2,c2
fid.close()
off(k1)
off(k2)
```

Additional Testing Notes

This appendix contains notes that were taken during testing that were not appropriate to include anywhere else, but provide completeness of information. Testing between rounds of irradiation took approximately 27 minutes, with 21 minutes of that being dedicated to loop gain measurement and 6 minutes of that being DC characterization. The time spent moving equipment is included in those estimates. At the start of the test, all of the circuits were irradiated for the time that should have deposited 1 krad (Si) of dose, but the power supply was off, so the circuits were not powered. Then the circuits were correctly irradiated with 1 krad (Si) of dose. Next, converter F was irradiated for approximately 700 rad (Si) of dose while the power switches to the other converters were left open, then the power supply was turned off while the irradiator was still on for about 36 seconds, and then the irradiator was turned off as well. After this, all of the BNC shorts were put in place (connecting the power switches for all of the converters) and the converters were correctly irradiated for the “1 krad (Si) to 2 krad

(Si)" dose step. All further irradiation steps were performed correctly. These mistakes were documented, but did not seem to have an impact on the results of the test. In some cases at relatively high total doses, a converter would be operating during irradiation (as seen by the current draw on the power supply) and then not function during small-signal characterization. In these cases, a measurement was performed and then the power was cycled and if the circuit returned to operation, then another measurement was recorded. In data sets that have two measurements, this is what happened and one of them is denoted with a "B" after the total dose.

DC Graphs

The body of the thesis presented Converter A and Converter D as examples of the responses for each of the configurations. This appendix provides the DC sweeps for all of the circuits for completeness. All circuits went through the DC characterization after every dose step. In the following figures, if all remaining DC sweeps are roughly zero volts, then only the first one is shown. In most cases, each sweep followed the same general shape with slight variation in the turn-on voltage and some increase in the output voltage, with increasing total dose. However, in some cases in Figure 59, the circuit partially turned on. Additionally, in Figure 63 and Figure 64 there were times when the circuitry designed to have the converter start in a prebiased output [22] did not function correctly. Instead of going from an output of approximately 0 V to the desired output voltage at the turn-on voltage, the output voltage gradually increased as the input voltage increased. This is not believed to be because of total dose though because these instances occurred during a few measurements at low doses and at high doses.

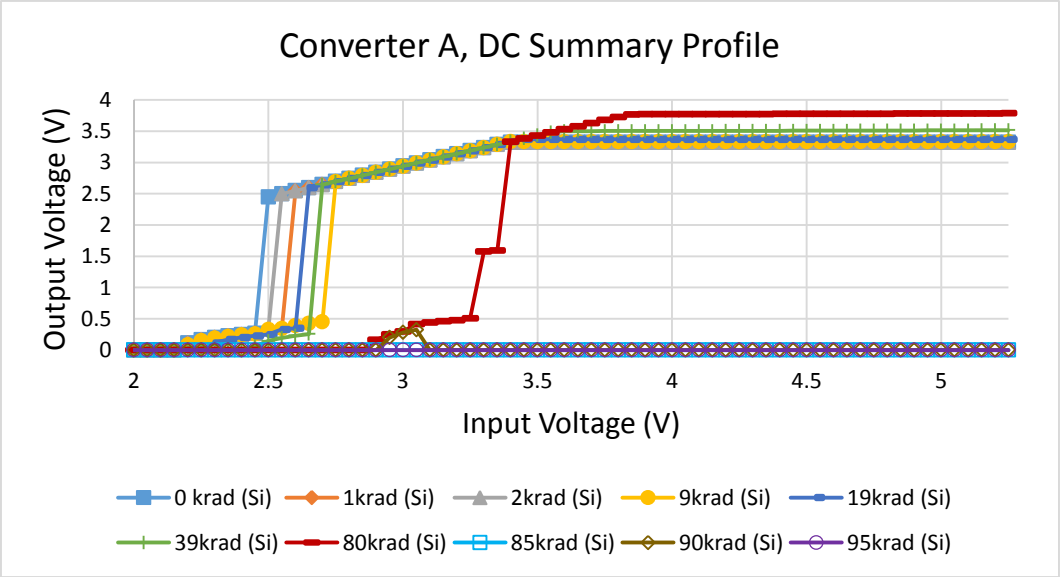

Figure 59. DC sweeps for Converter A, Configuration 1

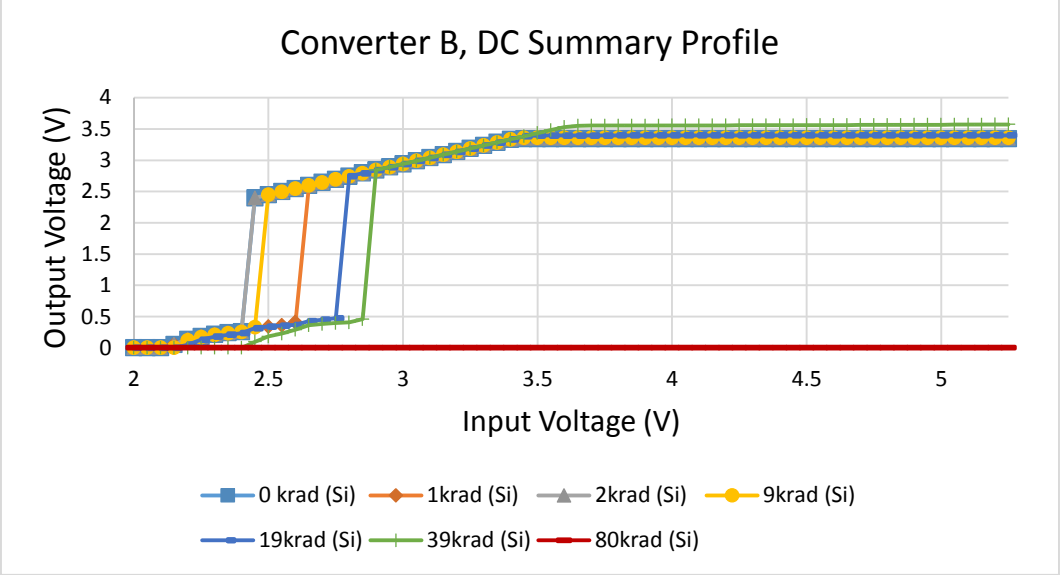

Figure 60. DC sweeps for Converter B, Configuration 1

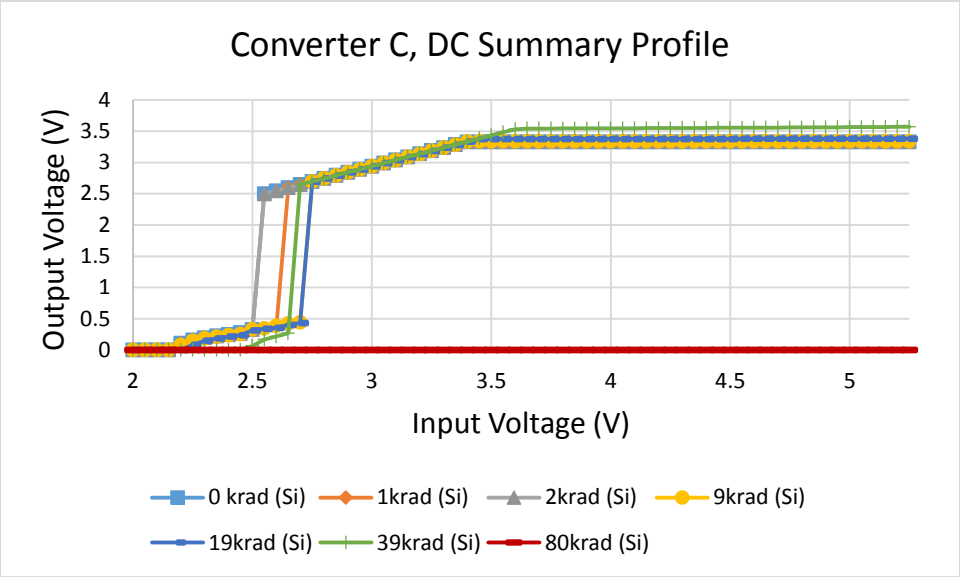

Figure 61. DC sweeps for Converter C, Configuration 1

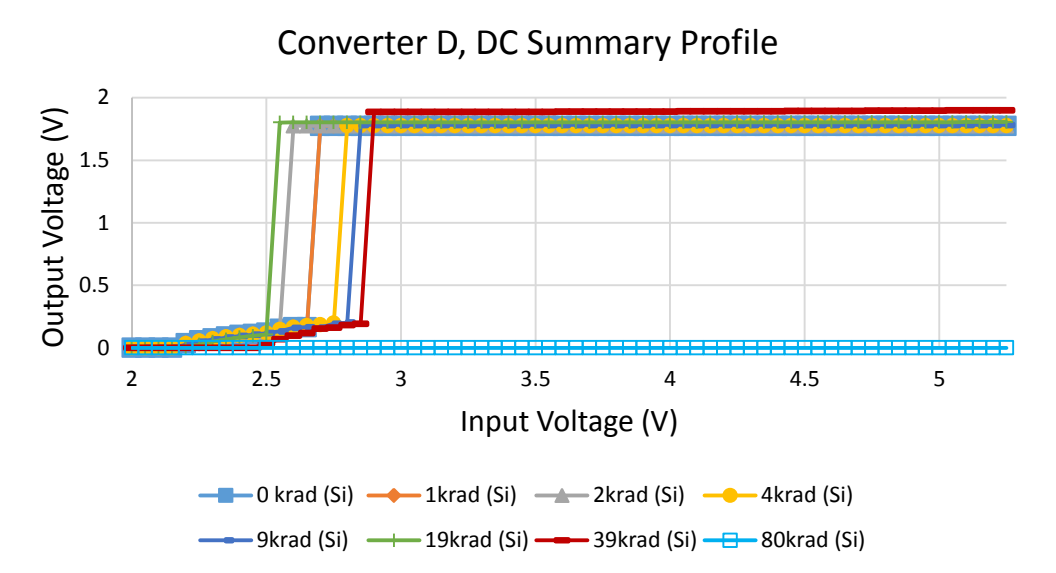

Figure 62. DC sweeps for Converter D, Configuration 2

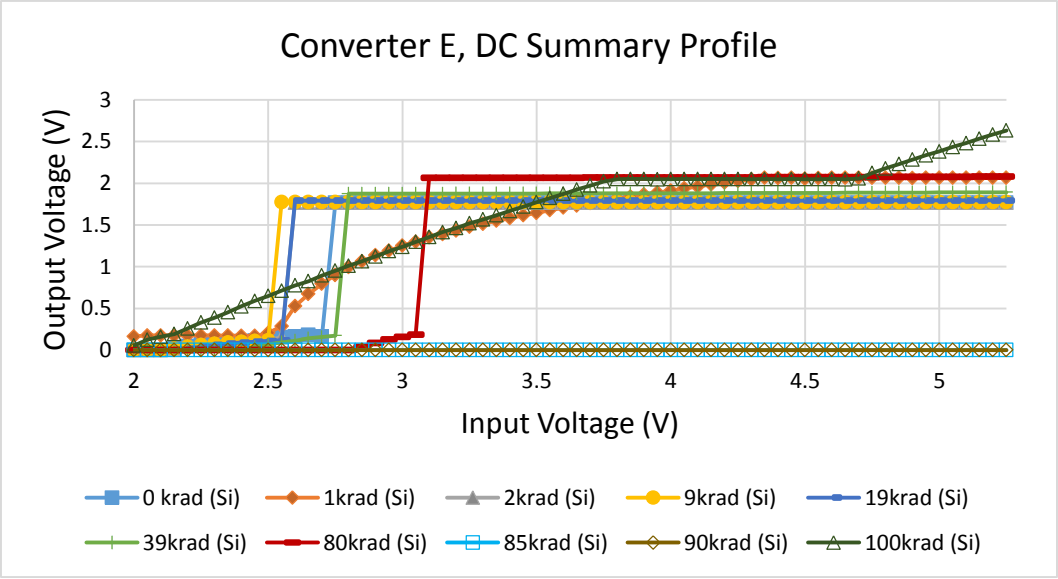

Figure 63. DC sweeps for Converter E, Configuration 2

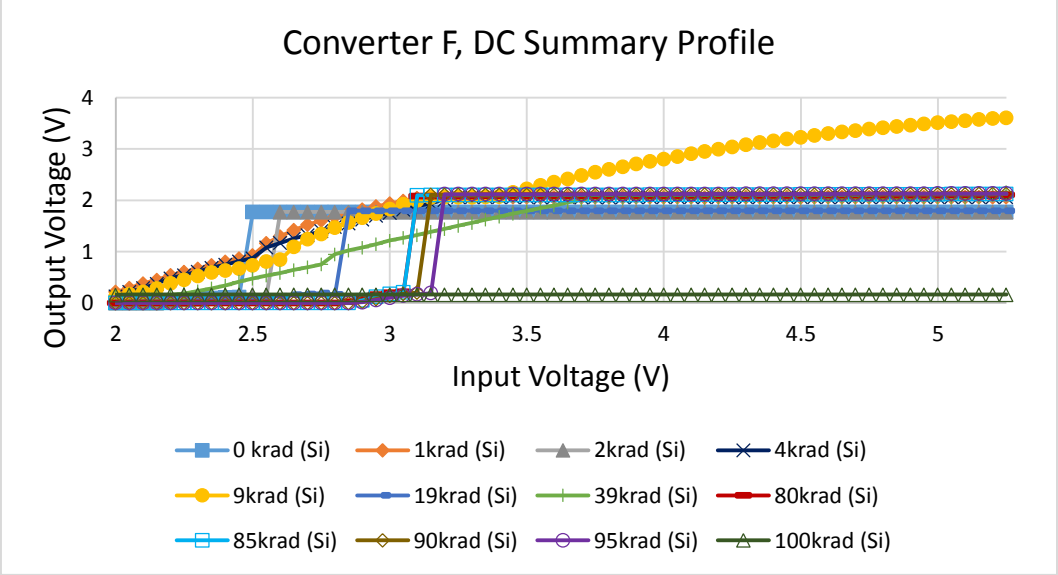

Figure 64. DC sweeps for Converter F, Configuration 2

Small Signal Graphs

Similar to the DC graphs, the small-signal graphs have been included for completeness. The loop gain, phase, and some graphs of some other small-signal quantities have been included.

Loop Gain

The importance of loop gain has been discussed in the body of this thesis. This section includes the loop gain data for all six converters for completeness. Converters B and C seemed to be biased on the edge of two different modes of operation and their loop gain curves changed when the switched between the modes (mode changes were seen by simultaneous changes in the LX voltages and inductor currents seen on the oscilloscope). All of the converters showed a significant decrease in loop gain that corresponded with regulation failure. The mode changes in converters B and C limit the ability to identify trends, but the other converters all show an increase in the loop gain/an increase in the crossover frequency corresponding with increasing dose prior to regulation failure. This trend is discussed further in the body of the thesis. Some of the converters displayed a failure loop gain curve (one that was below the 0 dB line), but then recovered after a power cycle. In these cases, both loop gain curves are included. Converter E even recovered during loop gain measurement, as shown by the 80 krad (Si) curve in Figure 73.

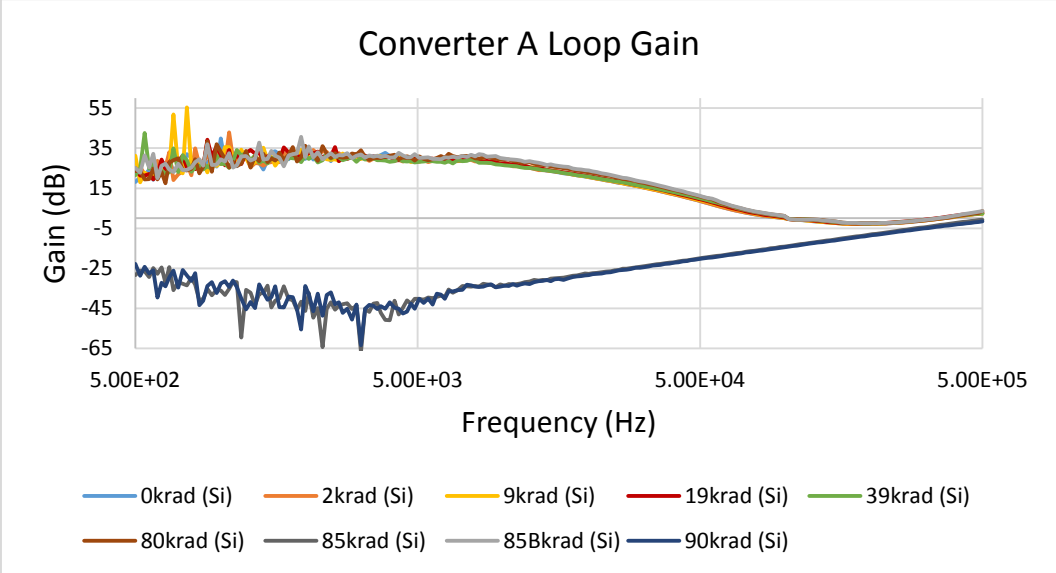

Figure 65. Converter A loop gain shows failure

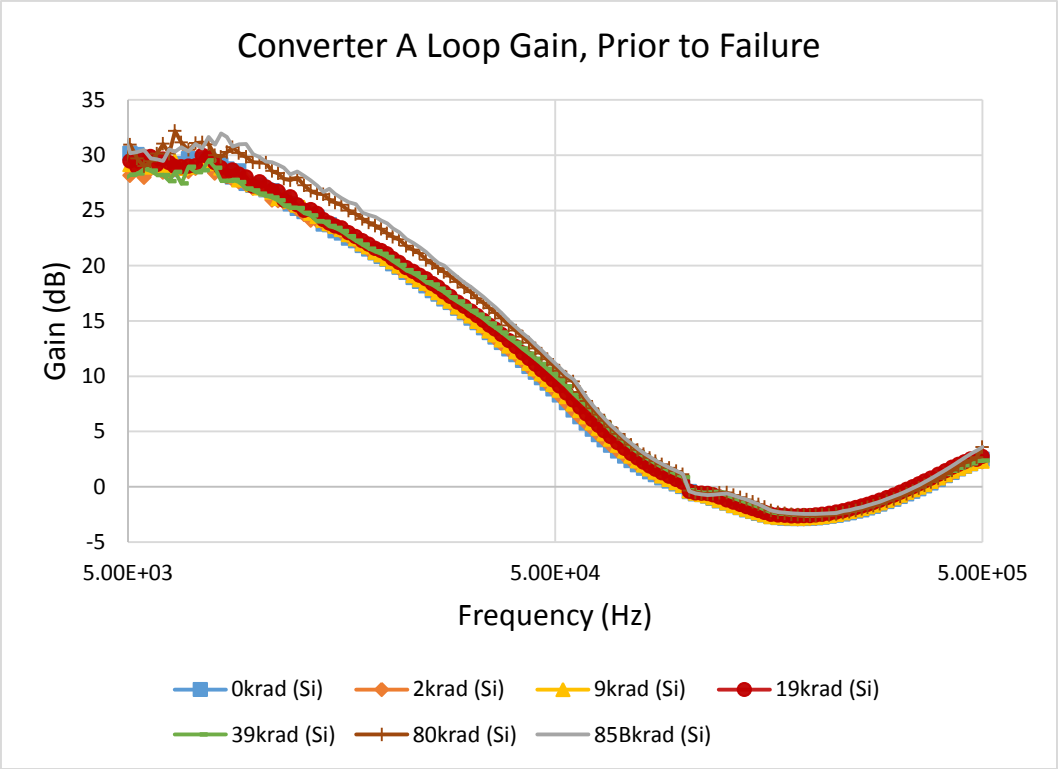

Figure 66. Converter A prior to failure shows small increases in loop gain with increasing total dose

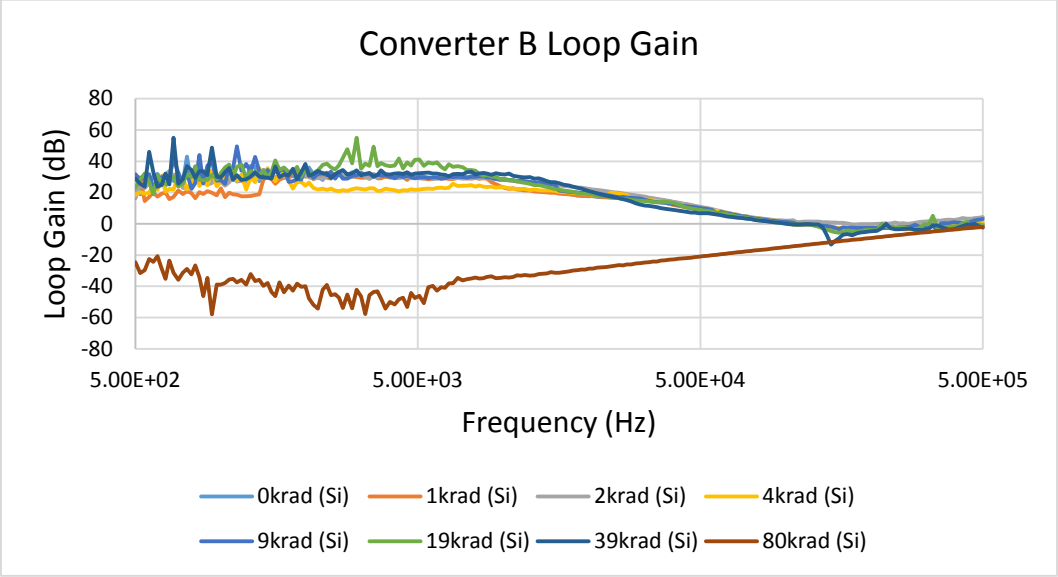

Figure 67. Converter B loop gain shows failure

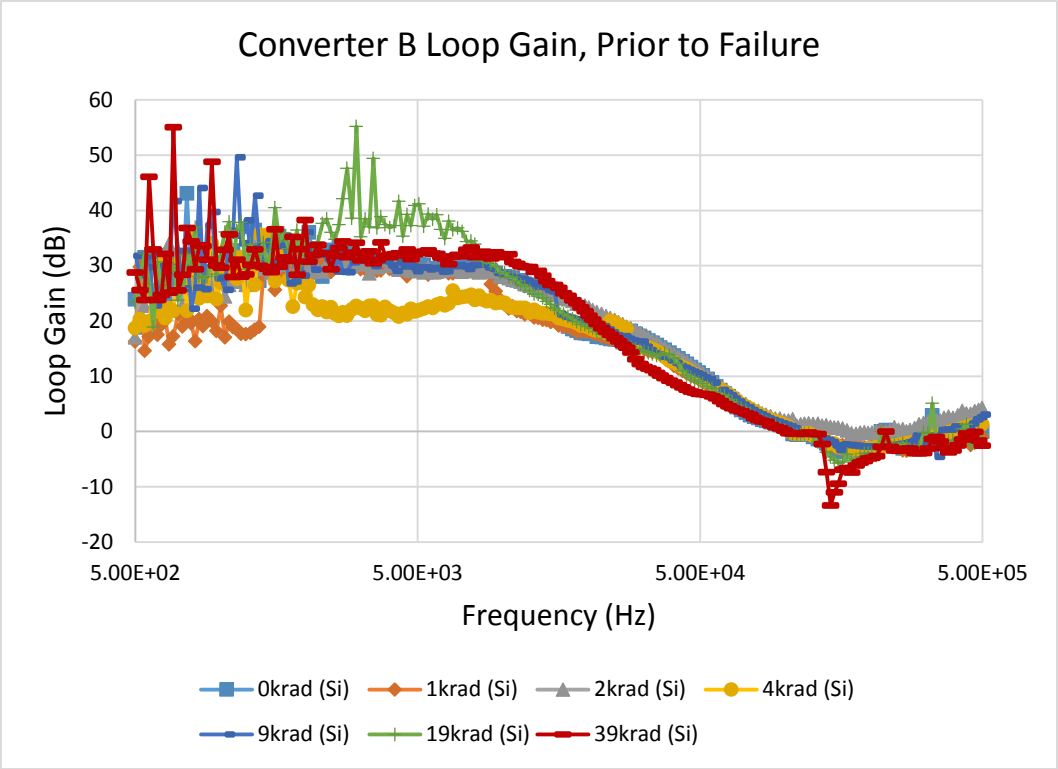

Figure 68. Converter B prior to failure shows changes in mode of operation

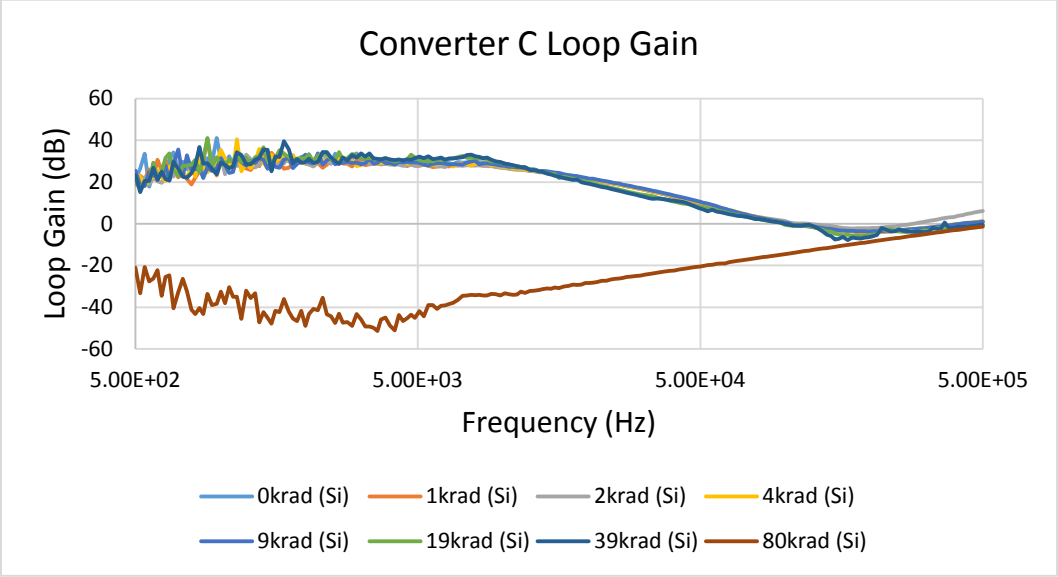

Figure 69. Converter C loop gain shows failure

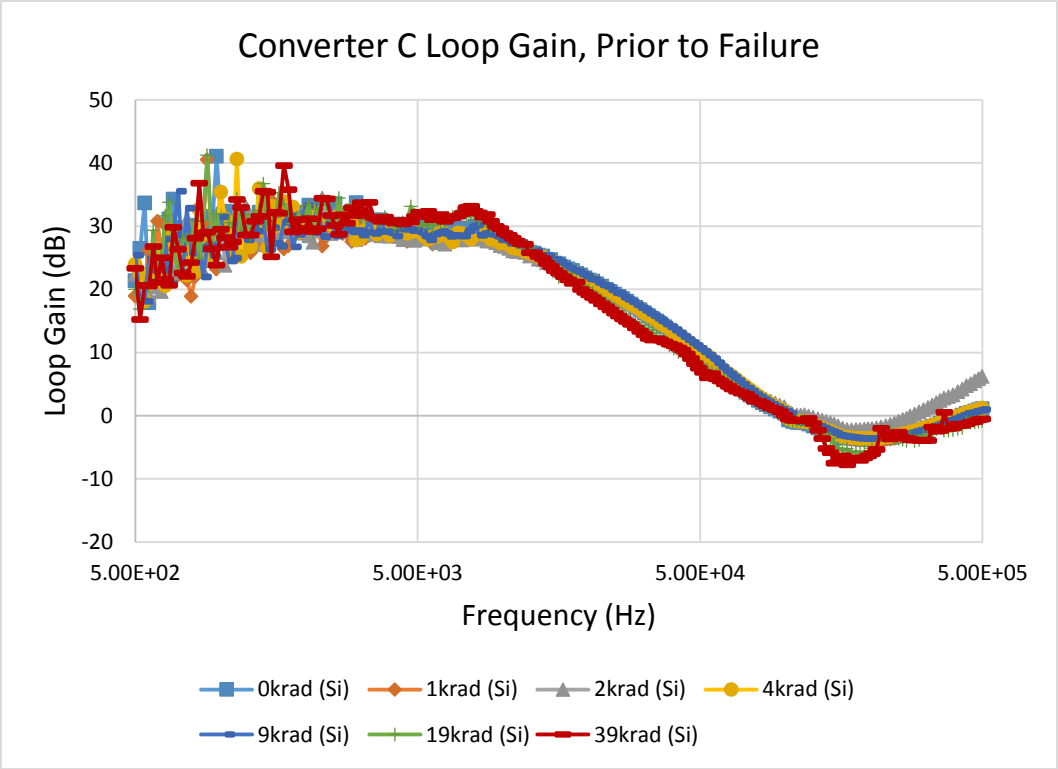

Figure 70. Converter C prior to failure shows some changes in mode of operation

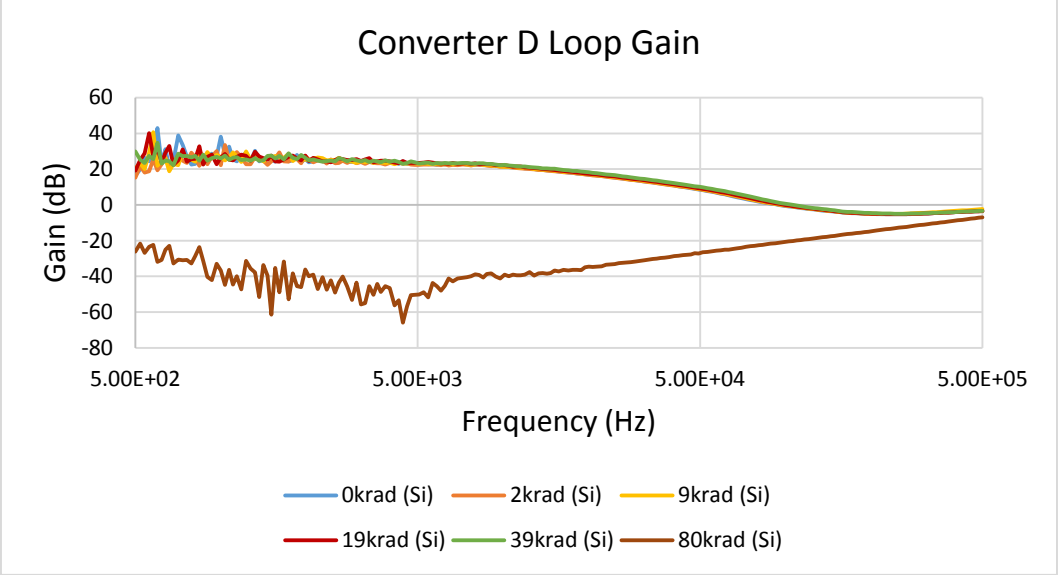

Figure 71. Converter D loop gain shows failure

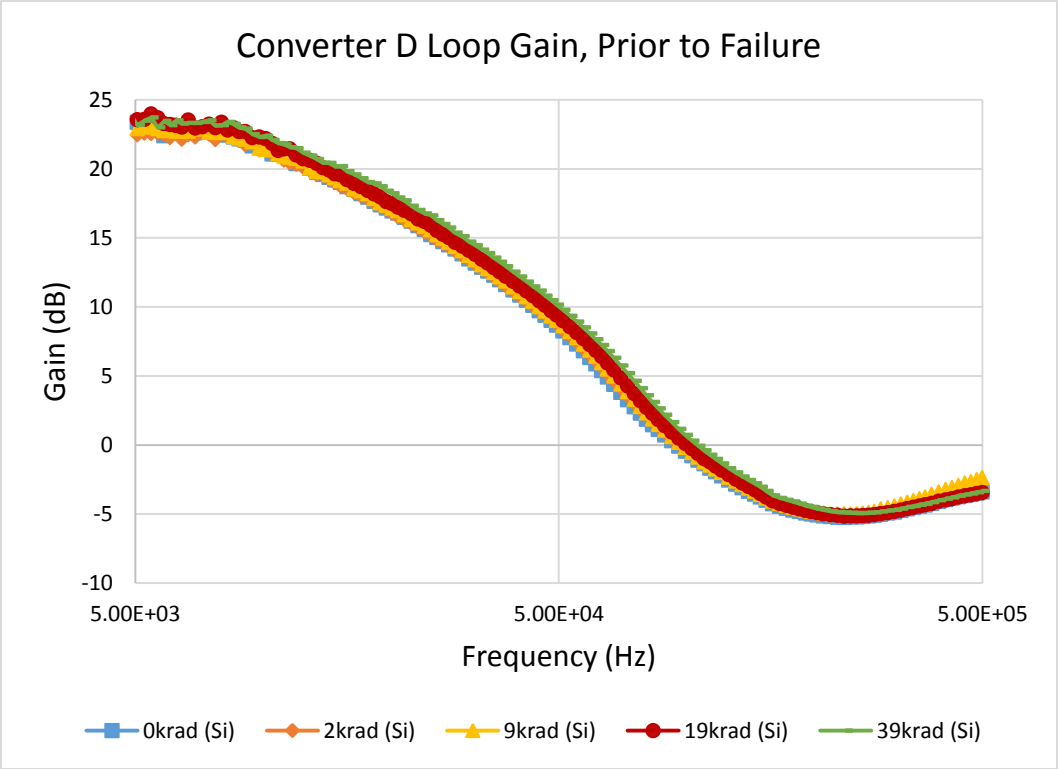

Figure 72. Converter D prior to failure shows small increases in loop gain with increasing total dose

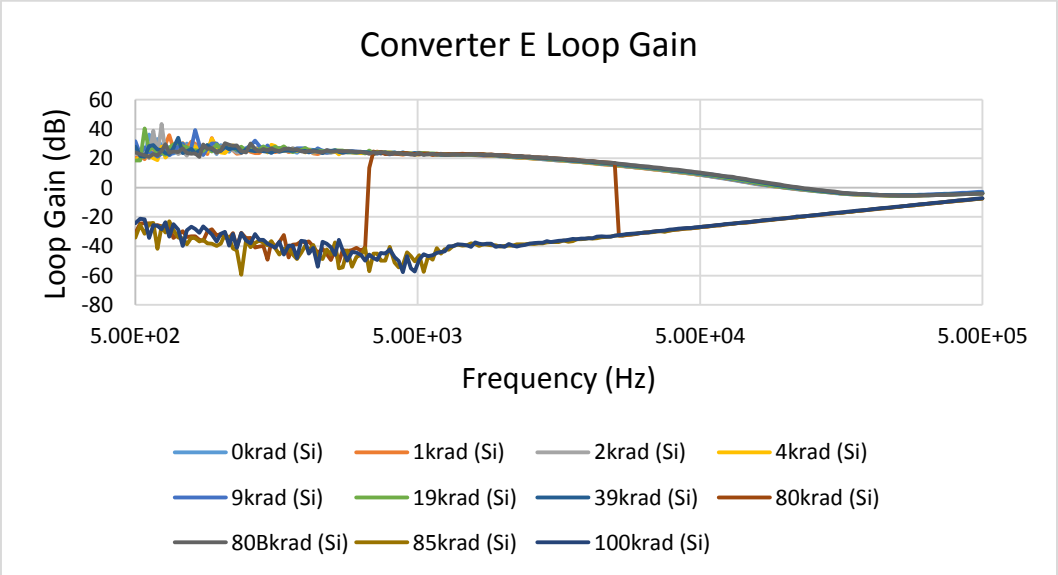

Figure 73. Converter E loop gain shows failure, and recovery

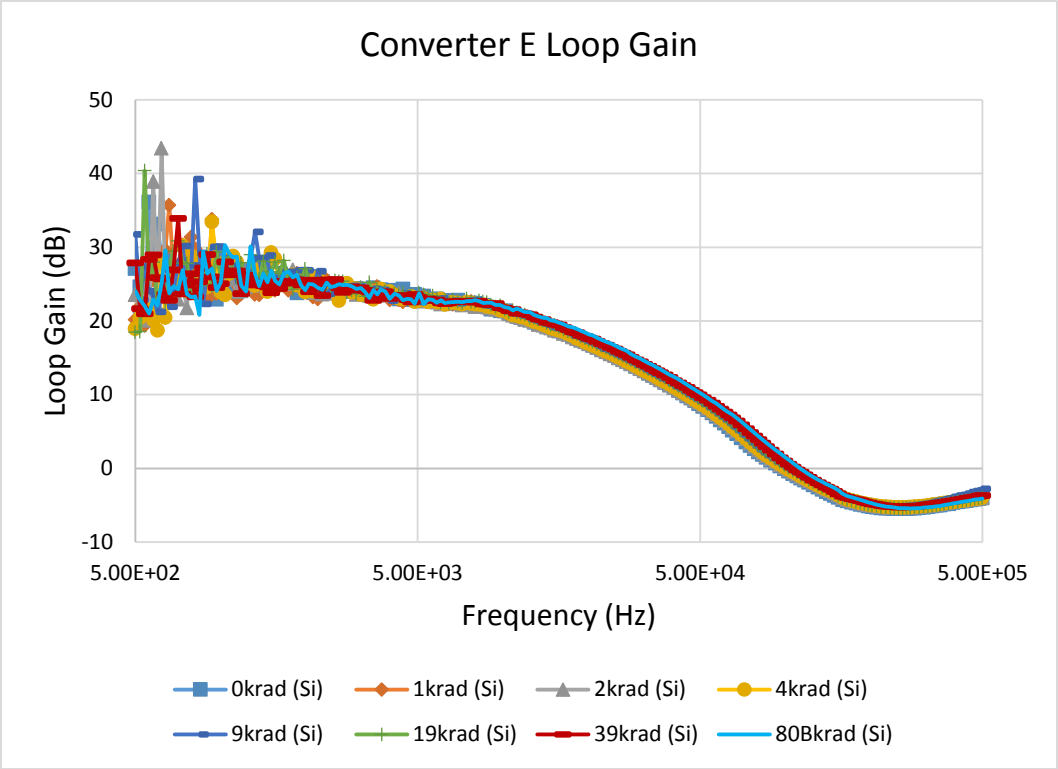

Figure 74. Converter E prior to failure shows small increases in loop gain with increasing total dose

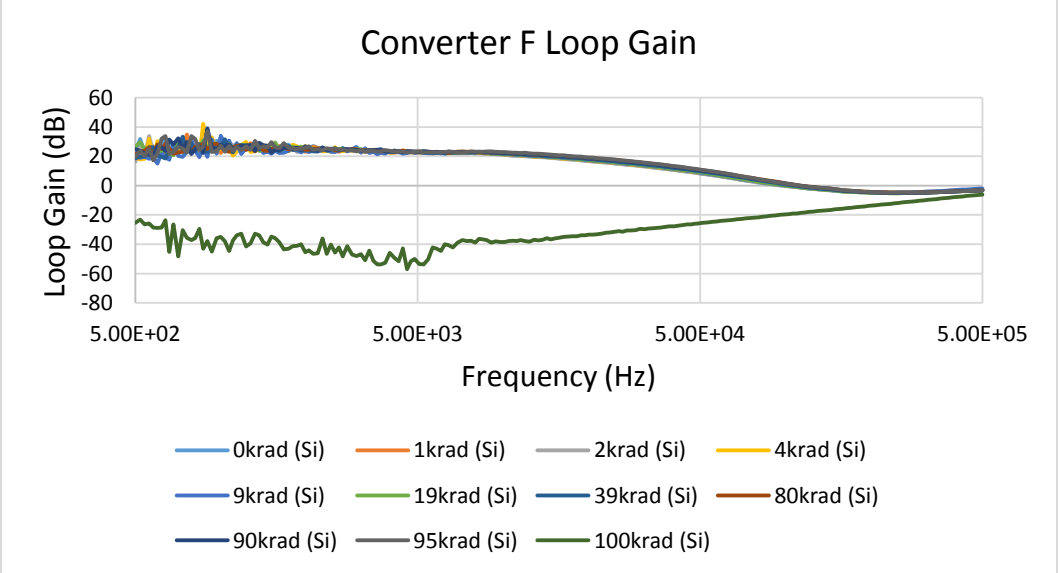

Figure 75. Converter F loop gain shows failure

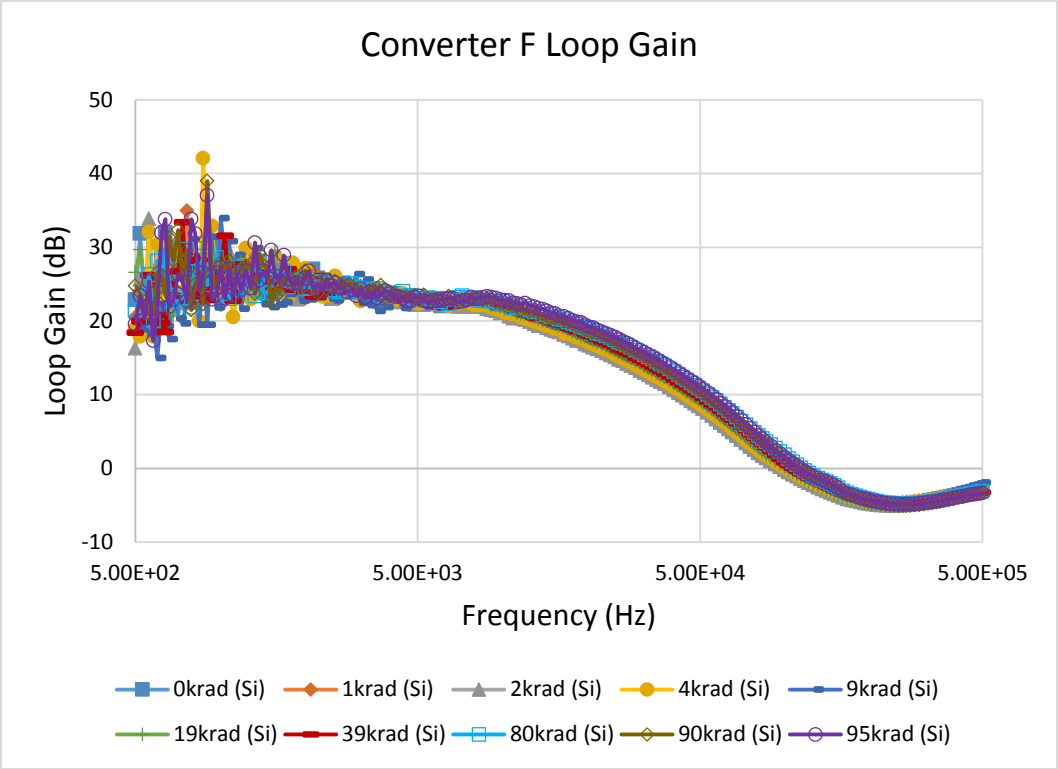

Figure 76. Converter F prior to failure shows small increases in loop gain with increasing total dose

Phase

Figure 77 - Figure 82 contain the phase data that corresponds with the loop gain data shown above. On its own, phase does not provide much information, but it is included so that someone could examine it someday if interested. Some more useful quantities that are derived from the loop gain and phase data – crossover frequency, phase margin, and gain margin – are provided after the phase data.

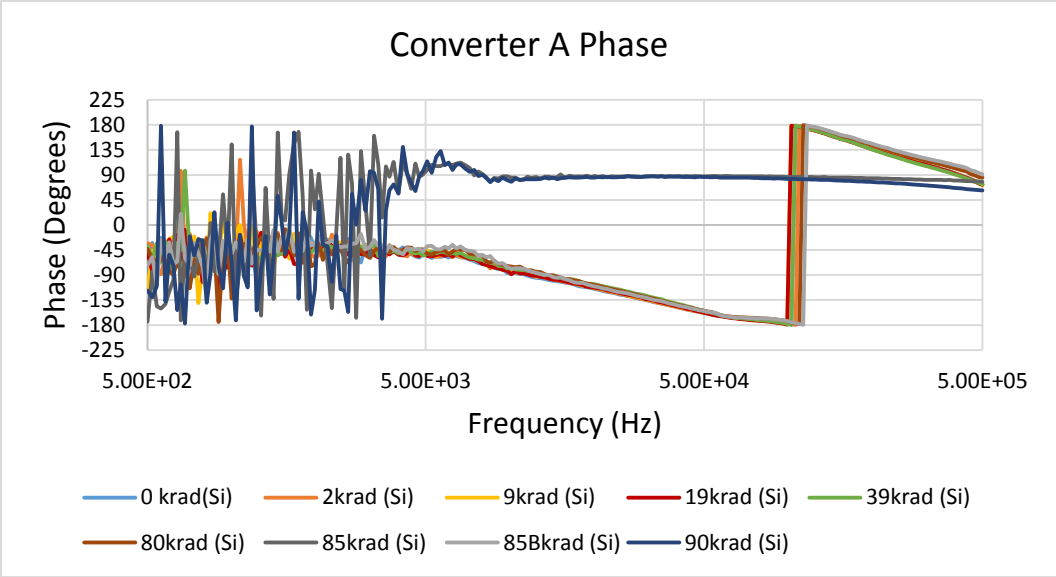

Figure 77. Converter A phase

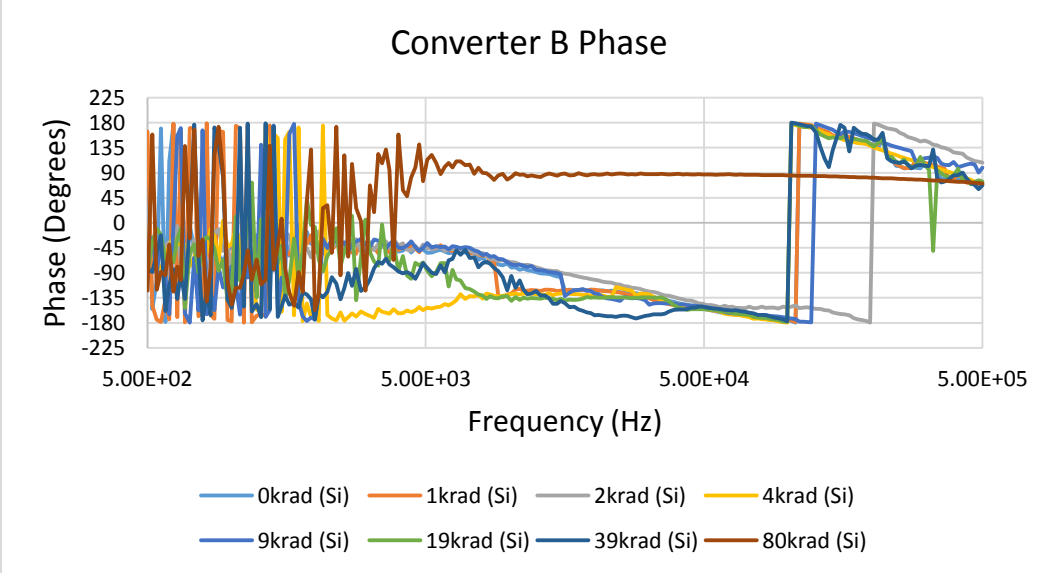

Figure 78. Converter B phase

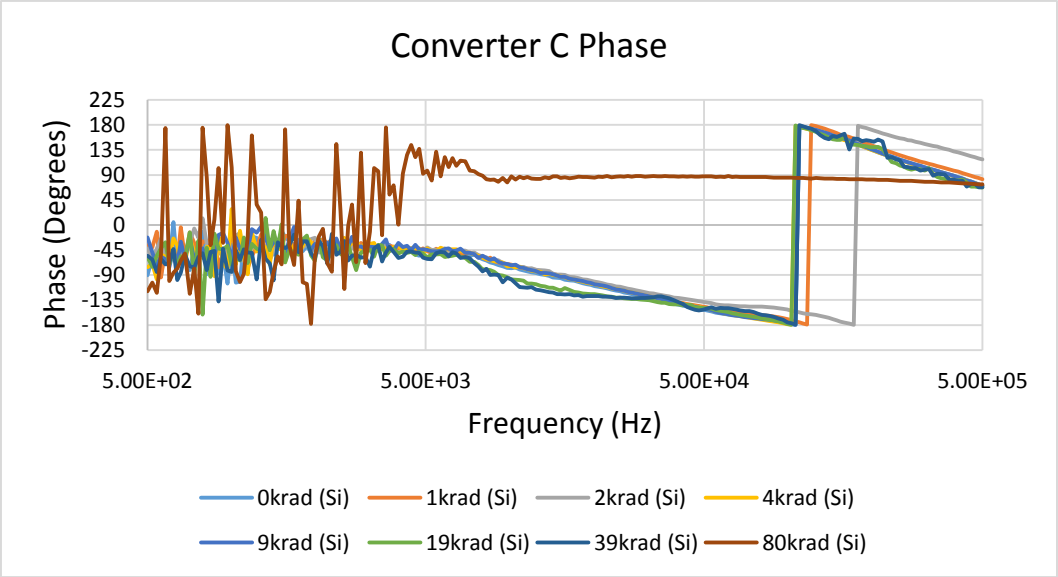

Figure 79. Converter C phase

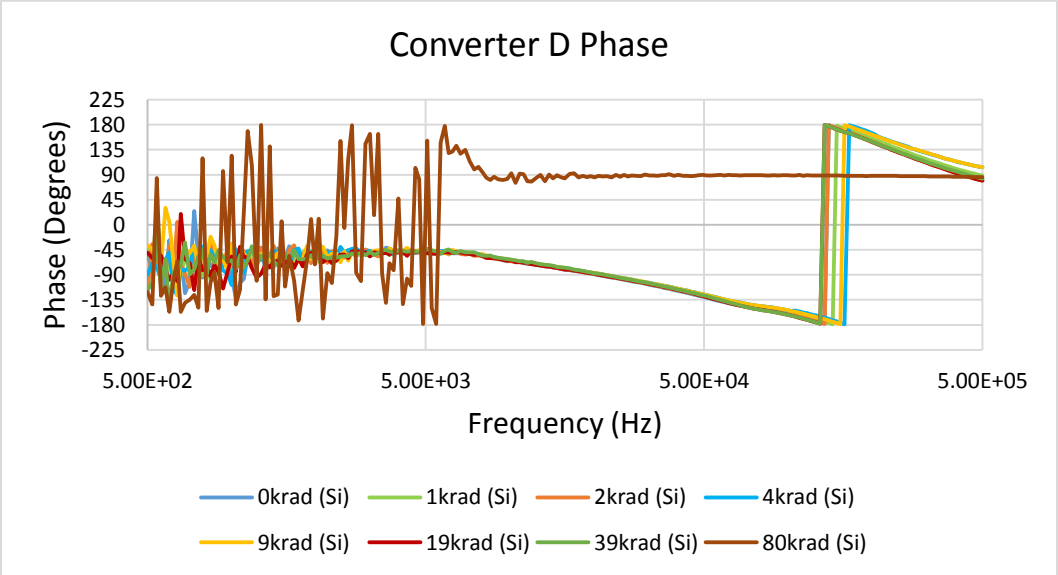

Figure 80. Converter D phase

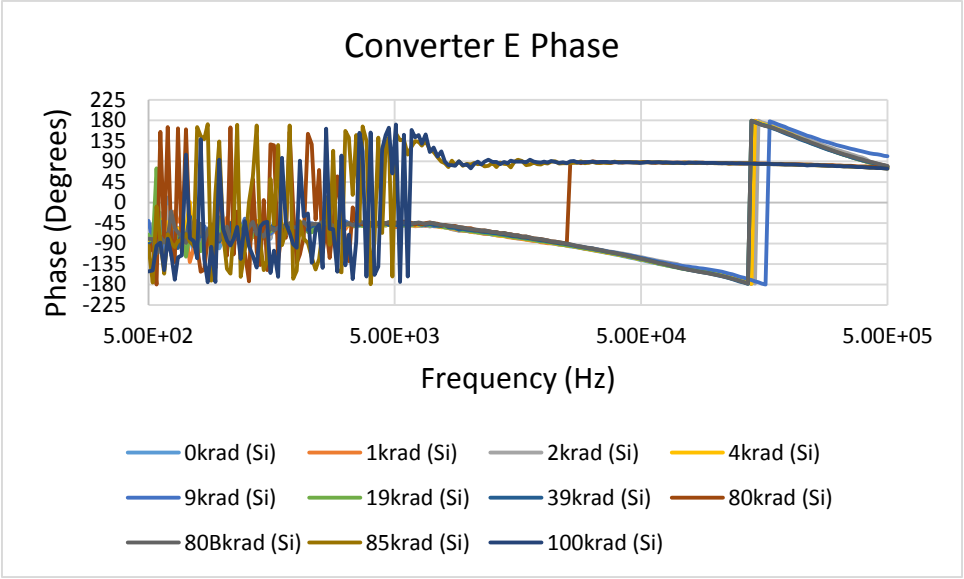

Figure 81. Converter E phase

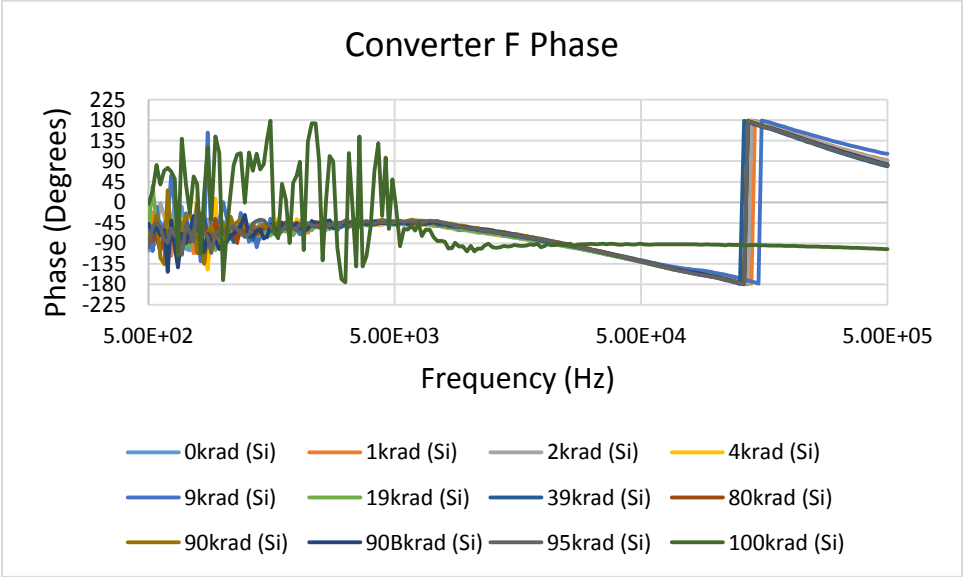

Figure 82. Converter F phase

Crossover Frequency

Figure 83 shows the crossover frequencies of the tested converters with increasing total dose. The crossover frequency is simply the frequency where the loop gain goes down to unity (0 dB). The data shows slightly increasing crossover frequencies prior to failure.

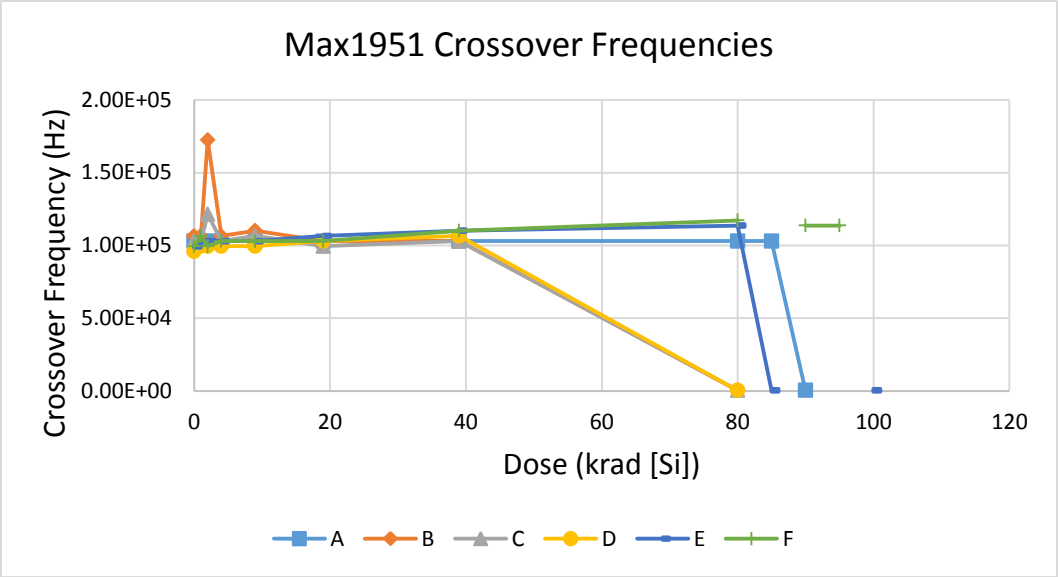

Figure 83. Crossover frequencies of the Max1951 converters versus dose

Phase Margin

The phase margin is the distance between -180 degrees and the phase at the crossover frequency, creating a measure of stability. Figure 84 shows the phase margins of the tested converters with increasing total dose. The data suggests decreasing phase margins prior to failure, but no definitive trend is present.

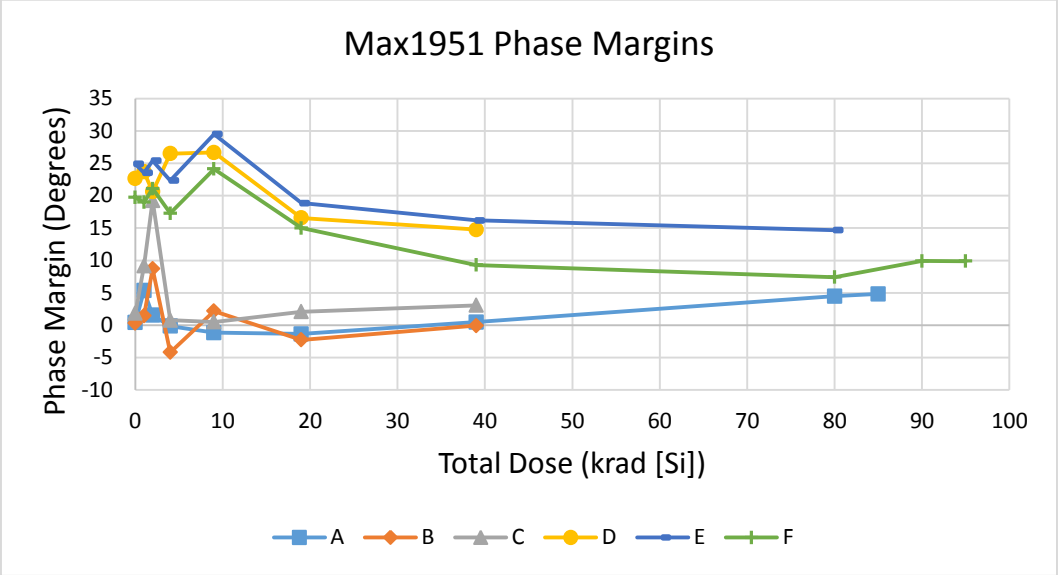

Figure 84. Phase margins of the Max1951 converters versus dose

Gain Margin

The gain margin is the magnitude of the gain at the crossover frequency, creating a measure of stability. If the gain margin is positive, then the converter is unstable. Figure 85 shows the gain margins of the tested converters with increasing total dose. The data suggests that the converters were stable (other than one point) prior to failure, but no definitive trend is present.

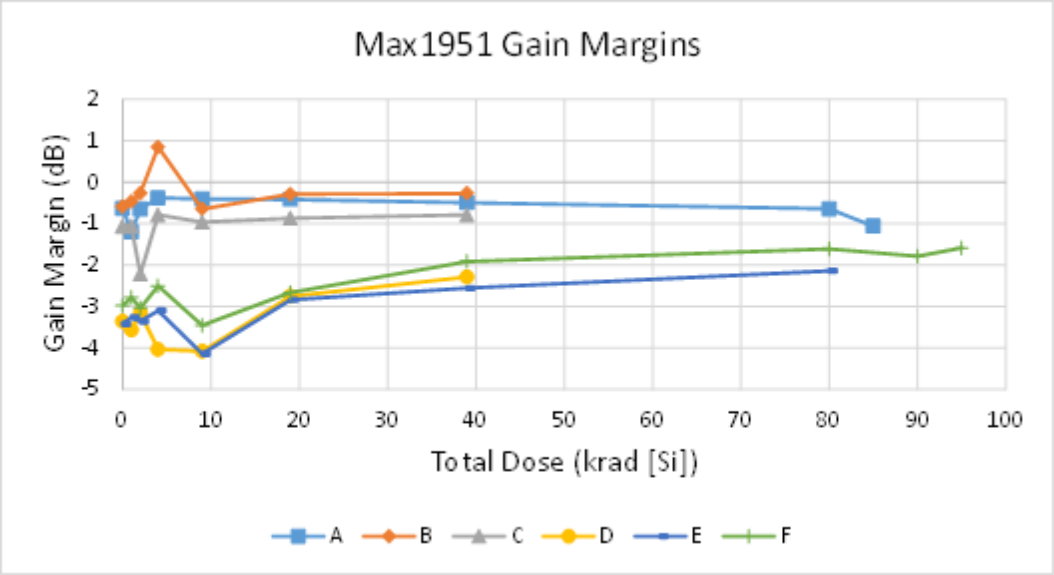

Figure 85. Gain margins of the Max1951 converters versus dose

Injection Circuit

Low frequency loop gain measurements provide valuable information about the DC regulation of the circuit. This test was limited in how low of a frequency accurate information could be obtained due to the limitations of the current probe used to inject the signal from the network analyzer into the test circuits. One solution to this problem would be to build an injection circuit that could accurately take the signal from the network analyzer and inject it into the test circuit. Figure 86 provides a schematic for a circuit designed to meet this goal. The use of two separate cores with different

permeabilities allows for a wider bandwidth since as the frequency response of one core decreases, the response of the other one increases. Such an injection circuit was built, and each of the separate components were tested separately and appeared to work. However, when the injection circuit was used as one unit to inject a signal, it did not function correctly. There appeared to be unstable feedback as the circuit would draw more current than expected and often produce sounds, appearing to push current through the cores in an oscillatory manner. The source of this problem was not found and is left for future work.

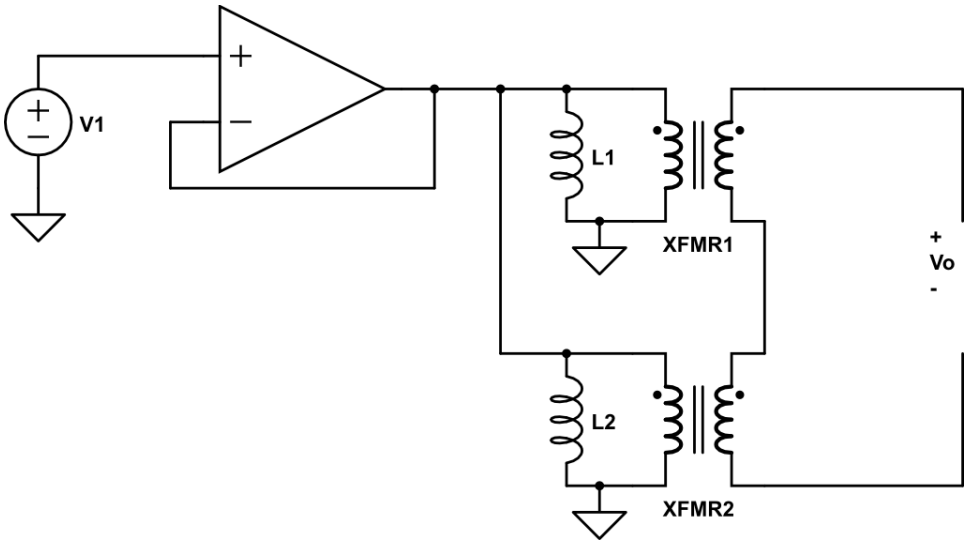

Figure 86. Injection circuit schematic

REFERENCES

[1] K. Nagatani, S Kiribayashi, Y. Okada, K. Otake, K. Yoshida, S. Tadokoro, T. Nishimura, T. Yoshida, E. Koyanagi, M. Fukushima, and S. Kawatsuma, "Emergency response to the nuclear accident at the Fukushima Nuclear Power Plants using mobile rescue robots," *Journal of Field Robotics*, vol. 30, no. 1, pp. 44-63, 2013.

[2] M. Swartwout, "CubeSat Database - swartwout," 25 March 2014. [Online]. Available: https://sites.google.com/a/slu.edu/swartwout/home/cubesat-database. [Accessed 17 June 2014].

[3] K. Nagatani,; Kiribayashi, S.; Okada, Y.; Tadokoro, S.; Nishimura, T.; Yoshida, T.; Koyanagi, E.; Hada, Y., "Redesign of rescue mobile robot Quince," *Safety, Security, and Rescue Robotics (SSRR), 2011 IEEE International Symposium on*, pp.13,18, 1-5 Nov. 2011

[4] K. Nagatani,; Kiribayashi, S.; Okada, Y.; Otake, K.; Kazuya Yoshida,; Tadokoro, S.; Nishimura, T.; Yoshida, T.; Koyanagi, E.; Fukushima, M.; Kawatsuma, S., "Gamma-ray irradiation test of electric components of rescue mobile robot Quince," *Safety, Security, and Rescue Robotics (SSRR), 2011 IEEE International Symposium on* , pp.56,60, 1-5 Nov. 2011

[5] A. Toorian, K. Diaz and S. Lee, "The CubeSat Approach to Space Access," *Aerospace Conference, 2008 IEEE*, pp.1,14, 1-8 March 2008

[6] D. M. Fleetwood, "Total Ionizing Dose Effects in MOS and Low-Dose-Rate Sensitive Linear-Bipolar Devices," *Nuclear Science, IEEE Transactions on* , vol. 60, no. 3, pp. 1706-1730, June 2013.

[7] R. W. Erickson and D. Maksimovic, Fundamentals of Power Electronics, Norwell, MA: Kluwer Academic Publishers, 2001.

[8] P.C. Adell, R.D. Schrimpf, B.K. Choi, W.T. Holman, J.P. Attwood, C.R. Cirba, and K.F. Galloway, "Total-dose and single-event effects in switching DC/DC power converters," *Nuclear Science, IEEE Transactions on* , vol.49, no.6, pp.3217-3221, Dec 2002.

[9] P.C. Adell, R.D. Schrimpf, W.T. Holman, J. Boch, J. Stacey, P. Ribero, A. Sternberg, and K.F. Galloway, "Total-dose and single-event effects in DC/DC converter control circuitry," *Nuclear Science, IEEE Transactions on* , vol.50, no.6, pp.1867,1872, Dec. 2003.

[10] A.T. Kelly, P.C. Adell, A.F. Witulski, W.T. Holman, R.D. Schrimpf, and V. Pouget, "Total Dose and Single Event Transients in Linear Voltage Regulators,"

Nuclear Science, IEEE Transactions on , vol.54, no.4, pp.1327,1334, Aug. 2007.

[11] A. S. Sedra and K. C. Smith, Microelectronic Circuits, New York: Oxford University Press, 2010.

[12] R. C. Dorf and R. H. Bishop, Modern Control Systems (12th Edition), Upper Saddle River, NJ: Prentice Hall, 2011.

[13] R. D. Middlebrook, "Measurement of loop gain in feedback systems," *Int. J. Electronics,* vol. 38, no. 4, pp. 485-512, 1975.

[14] R. D. Middlebrook, "The GFT: A Final Solution for Design-Oriented Feedback Analysis," Ardem Associates, San Dimas, CA, 2004.

[15] J. L. Barth, "Space, atmoshperic, and terrestrial radiation environments," *Nuclear Science, IEEE Transactions on* , vol. 50, no. 3, pp. 466-482, 2003.

[16] L. Massengill, "SEU Modeling and Prediction Techniques," in *1993 NSREC Short Course*, Nashville, 1993.

[17] J. R. Srour, C. J. Marshall and P. W. Marshall, "Review of Displacement Damage Effects in Silicon Devices," *Nuclear Science, IEEE Transactions on,* vol. 50, no. 3, pp. 653-670, 2003.

[18] P. J. Wahle, R. D. Schrimpf and K. F. Galloway, "Simulated Space Radiation Effects on Power MOSFET's in Switching Power Supplies," *Industry Applications, IEEE Transactions on* , vol. 26, no. 4, pp. 798-802, 1990.

[19] J. Pizano, T. Ma, J. Attia, R. Schrimpf, K. Galloway and A. Witulski, "Total dose effects on power-MOSFET switching converters," *Microelectronics Reliability,* vol. 38, pp. 1935-1939, 1998.

[20] P. C. Adell, R. D. Schrimpf, W. T. Holman, J. L. Todd, S. Caveriviere, R. R. Cizmarik and K. F. and Galloway, "Total Dose Effects in a Linear Voltage Regulator," *Nuclear Science, IEEE Transactions on,* vol. 51, no. 6, pp. 3816-3821, 2004.

[21] R. Burt, "Distributed Electrical Power System in Cubesat Applications," Logan, Utah, 2011.

[22] Maxim Integrated Products, *MAX1951A Application Note*, Sunnyvale, CA, 2009.

[23] Maxim Integrated Products, *MAX1951/MAX1952 Application Note,* Sunnyvale, Ca,

2009.